Lab on a Chip

RSC Publishing

PAPER

View Article Online
View Journal

A nanoliter-scale open chemical reactor†

Jean-Christophe Galas,* Anne-Marie Haghiri-Gosnet and André Estévez-Torres*

Cite this: DOI: 10.1039/c2lc40649g

An open chemical reactor is a container that exchanges matter with the exterior. Well-mixed open chemical reactors, called continuous stirred tank reactors (CSTR), have been instrumental for investigating the dynamics of out-of-equilibrium chemical processes, such as oscillations, bistability, and chaos. Here, we introduce a microfluidic CSTR, called μCSTR, that reduces reagent consumption by six orders of magnitude. It consists of an annular reactor with four inlets and one outlet fabricated in PDMS using multi-layer soft lithography. A monolithic peristaltic pump feeds fresh reagents into the reactor through the inlets. After each injection the content of the reactor is continuously mixed with a second peristaltic pump. The efficiency of the μCSTR is experimentally characterized using a bromate, sulfite, ferrocyanide pH oscillator. Simulations accounting for the digital injection process are in agreement with experimental results. The low consumption of the μCSTR will be advantageous for investigating out-of-equilibrium dynamics of chemical processes involving biomolecules. These studies have been scarce so far because a miniaturized version of a CSTR was not available.

Received 7th June 2012,
Accepted 7th November 2012

DOI: 10.1039/c2lc40649g

www.rsc.org/loc

1. Introduction

The systemic view of biological processes has regained strength with the advent, in the last twenty years, of powerful instrumental techniques such as genotyping,[1] fluorescent proteins,[2] or high performance microscopy.[3] Throughout the process it has been shown experimentally that many of the complex behaviours that we marvel at in living cells are controlled by networks of chemical reactions: gene networks, signalling protein networks and metabolic networks.[4–6] These networks are maintained out of equilibrium and their functional response depends on two characteristics: their topology, *i.e.* how many nodes there are and which is connected to which, and their coupling strengths, *i.e.* what dynamics link two nodes. It appears that the topology may be determined experimentally[7] but measuring the rates of the chemical process linking two nodes is much more difficult. We anticipate that studying the dynamics of purified biological networks in highly controlled environments outside of cells will help to understand how complexity emerges in biology.[8] Moreover, synthesizing *in vitro* networks with diverse dynamic behaviours is expected to open new endeavours in material sciences and in molecular computation,[9] *i.e.* assemblies of molecules that are able to process information and make non-trivial decisions depending on their environment.

The discipline of non-linear chemistry has, from the 1970s to the 1990s, provided a rigorous theoretical corpus and a sheer diversity of experimental observations on the dynamics of chemical systems far from equilibrium.[10] The systems studied in non-linear chemistry are networks of inorganic chemical reactions, principally variations around the classical Belousov-Zhabotinsky oscillator. In contrast to biological reaction networks, we have a good mechanistic description of these inorganic systems and a precise measurement of their dynamic rates. First, this is because inorganic networks are significantly smaller and second, it is simpler to measure concentrations and rate constants of chemical species within tubes than inside living cells. However, inorganic reactions are hard to assemble in networks with predefined dynamic behaviours and, in this regard, synthetic biology has done better than inorganic chemistry.[11,12] In the last ten years an intermediate strategy has emerged. It harnesses the predictable reactivity of certain biomolecules, notably nucleic acids and enzymes, to assemble reaction networks with controlled dynamic behaviours outside of cells. This direction was started by the seminal paper of Yurke and coworkers[13] and reached a landmark in 2011 when Rondelez and Winfree, together with their coworkers, independently synthesized the first engineered chemical system that is able to oscillate in a closed reactor.[14,15]

To study the dynamics of either purified biological networks or synthetic reaction networks using biomolecules one needs an open chemical reactor that keeps the system far from equilibrium. In this regard, microfluidics is the technology of choice because it provides a precise spatiotemporal[16,17] control of the concentrations of reagents with, typically, 1 μm and 1 s

Laboratoire de photonique et de nanostructures, CNRS, route de Nozay, 91460 Marcoussis, France. E-mail: Jean-Christophe.Galas@lpn.cnrs.fr; aestevez@lpn.cnrs.fr

† Electronic Supplementary Information (ESI) available. See DOI: 10.1039/c2lc40649g

resolution. Microfluidics has, however, stayed relatively quiet in the development of tools for studying far-from-equilibrium chemical systems. In 2004 Ginn *et al.* were the first to study chemical waves within microfluidic devices.[18] In a series of remarkable papers, Ismagilov and collaborators coupled microfluidic design and non-linear inorganic reactions to artificially mimic the spatio-temporal dynamics of blood clotting.[19,20] More recently, Epstein and collaborators encapsulated the Belousov-Zhabotinsky reaction into arrays of water-in-oil droplets and showed the spatial coupling of these microreactors through the diffusion of bromine, which is soluble in the oil phase.[21] A miniaturized version of the continuous stirred tank reactor (CSTR), an open reactor that revolutionized the investigation of non-linear chemical reactions ,[22–24] has never been demonstrated. The implementation of such a device is the objective of this work: we used an annular reactor, with injection and mixing actuated through monolithic PDMS microvalves,[25,26] to study the dynamics of a pH oscillator. Our miniaturized open reactor brings the possibility to study reaction networks involving biomolecules (whether endogenous or synthetic) to explore the interesting dynamic behaviours that lie far from equilibrium. Throughout the text we use the term open reactor as it is employed in chemical engineering: a container that exchanges matter with the external world.[27]

2. Principle of the μCSTR

A continuous stirred tank reactor (CSTR), depicted in Fig. 1A, is an open reactor fed through two or more inlets with reagents i at concentrations C_i^{IN} and at a flow rate Q (Ls^{-1}). The reactor, of volume V, is supposed to be perfectly stirred, such that each infinitesimal injection of fresh reagents is instantaneously homogenised in the whole reactor. The outlet discards reagents at concentration $C_i(t)$ and flow rate Q, thus keeping V constant. Millilitre-scale CSTRs are useful in the study of chemical oscillators as a simple way to maintain a chemical reaction out of equilibrium.[23] A key parameter of the CSTR is the residence time of the reagents inside the reactor, $\tau_R = V/Q$, or its inverse, the feeding rate, $k_0 = \tau_R^{-1}$. The temporal evolution of the concentration of species i in the CSTR is thus written

$$\frac{dC_i(t)}{dt} = f_i(k_j, C_l(t)) + k_0(C_i^{IN} - C_i(t)) \quad (1)$$

Where the function $f_i(k_j, C_l(t))$, derived from the law of mass action, accounts for concentration variations due to chemical reactions, k_j being the rate of chemical reaction j ($j \neq 0$), and the index l spans all species that consume or produce species i. This equation illustrates the principal interest of using a CSTR: the physical parameter k_0, that can be easily tuned experimentally, plays the role of a first-order reaction rate and provides an extra degree of freedom to explore chemical dynamics far from equilibrium.

In the implementation of a microfluidic version of a CSTR (μCSTR) one has to solve two issues: (i) how to control k_0, *i.e.* the flow rate, and (ii) what mixing strategy will be chosen. We have identified three possible experimental implementations of a μCSTR: (i) an open reactor with diffusive mixing containing no active fluidic parts, (ii) a droplet reactor with digital injection, and (iii) an annular open reactor with digital injection and forced mixing, involving valves and pumps. In the diffusion reactor, both the mixing time and the feeding rate depend on the diffusion coefficient of the different molecules, which is impractical. An elegant droplet-based open reactor has been recently proposed by Takinoue and coworkers,[28] but it has not yet been used to study chemical reactions, as we show here. Another implementation of the droplet reactor could use electrowetting on dielectric technology (EWOD),[29] although with significantly larger volumes, 0.1 to 1 μL. The annular open reactor is discussed in this paper.

3. Results and discussion

3.1. Description of the device

The μCSTR developed in this work is displayed in Fig. 1 and its fabrication is described in Methods. Flow channels appear in

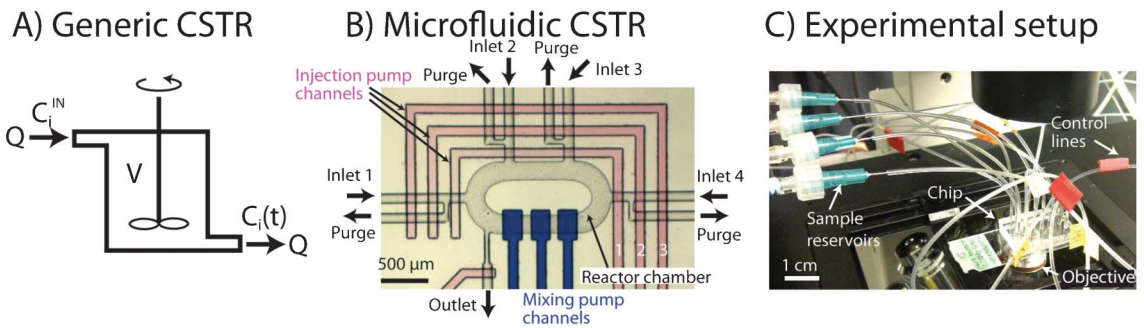

Fig. 1 Microfluidic continuous stirred tank reactor (μCSTR). (A) Scheme of a generic CSTR of volume V. Species i is injected at concentration C_i^{IN} and flow rate Q and ejected at concentration $C_i(t)$ and at the same flow rate. The concentration of i inside the reactor is always homogeneous and equal to $C_i(t)$ due to perfect mixing. (B) Brightfield photograph of the μCSTR with flow channels in grey and control channels in colour. The three channels of the injection pump appear in red, together with that of the outlet valve. Channels for the mixing pump appear in blue. Fresh reagents may be injected into the annular reactor or flushed into the purge channels (injection valve 1 closed). (C) The μCSTR chip on the microscope stage connected to sample reservoirs and control pressure lines.

grey and are at the bottom layer of the chip. They are 10 μm high and have a rounded section. Control channels appear in red or blue and are at the top layer of the chip. They are 50 μm high. The red and blue channels actuate the peristaltic injection and mixing pumps, respectively. The reactor is an annular channel 200 μm wide and with a major axis of 1.5 mm. Four 100 μm wide inlet channels carry fresh reagents into the reactor through the peristaltic injection pump. When the injection plug is pushed into the reactor the outlet valve is open. After every injection event, the injection valve 1 and the outlet valve are closed, to isolate the reaction chamber, and the mixing pump is actuated continuously at 4 Hz. During this time, injection valves 2 and 3 are open and fresh sample flows from the inlet channels into the purge channels. This continuous purge of fresh reagents was implemented to prevent the degradation of the bromate solution; otherwise the pH of the bromate inlet channel rapidly dropped from its normal value at pH 7 to pH 3 or lower (see ESI, Fig. S6†).

3.2. Characterization of the injection and determination of the feeding rate

In the μCSTR, the feeding rate is given by

$$k_0 = \frac{Nv}{t_P V} = \frac{\beta}{t_P} \quad (2)$$

where N is the number of inlets, v is the volume injected at one inlet, t_P is the injection period and V is the volume of the reactor. $\beta = Nv/V$ is the relative volume of a single injection event. To quantify v we acquired images every 250 ms during the injection of a slowly-diffusing fluorophore, 1 μM BSA-FITC mixed with unlabelled 100 μM BSA in 50 mM borate buffer pH 9.3, (Fig. 2A). Supposing that the height of the annular reactor is constant along its section, the volume of one injection is given by the product of the surface of the fluorescent spot injected, s, and the height of the reactor. In other words, the relative volume of injection is given by the ratio of s over the surface of the reactor S. However, the reactor channel has a rounded section, which is necessary for the valves to work properly.[25] To take this into account, we measured the dimensions of the reactor by recording the 3D profile of the μCSTR mould using a profilometer (see ESI, Fig. S3†). The injection volume measured for each inlet is summarized in Table 1. These values are consistent with the fact that, at each injection, we push twice the volume underneath the crossing between a control channel and an injection channel, 0.14 nL in our case. The volume injected through inlets 2 to 4 is the same within an experimental error of 15%, and equal to 0.15 nL. Injection through inlet 1 resulted in an injected volume that is 25% larger, probably due to a lower hydrodynamic resistance as it is close to the outlet. The total volume of the reactor is 5.2 ± 0.3 nL. In the following, we will retain v = 0.15 nL, constant for all four inlets, for calculating k_0. Thus, the relative volume of the reactor refreshed at each injection is β = 0.12. An experiment performed at a given k_0 means that injections were separated by an interval t_p, as calculated from eqn (2).

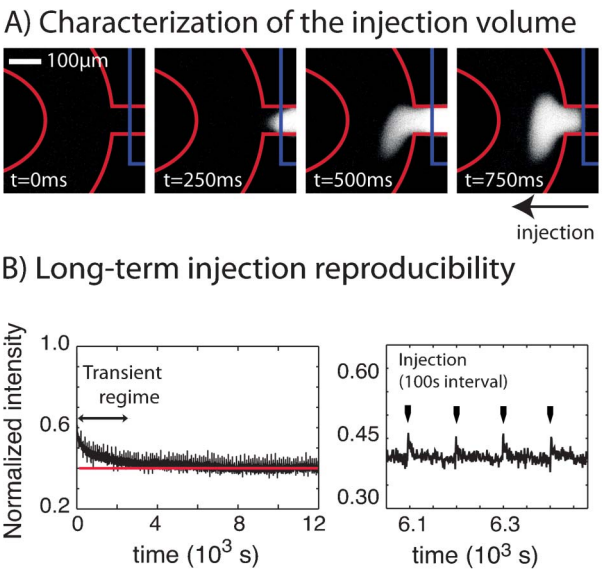

Fig. 2 Characterization of the injection in the μCSTR. (A) Time-lapse fluorescence images during the injection of 1 μM BSA-FITC, the boundaries of the reactor and the injection valve appear in red and blue, respectively. (B) Normalized average fluorescence intensity inside the reactor over 3.3 h during the injection of an unreactive mixture, the red line is a guide to the eyes. Non-fluorescent BSA and fluorescent BSA-FITC were injected every 100 s through inlets 1–3 and 2–4, respectively.

The investigation of the dynamic behaviour of the chemical oscillator described below required repetitive injections of reagents over long periods of time. For a given value of t_P an experiment lasted 2 h. We scanned sequentially 9 values of t_P overnight, the final conditions of run n being the initial conditions of run n + 1, resulting in about 700 injections at each inlet. Fluorescence images were captured every 1 s, using an automatic shutter to minimize photobleaching, which remained negligible. To test the reproducibility of the injection we recorded the average fluorescence inside the reactor when two non-reactive species were injected. Fig. 2B shows the average fluorescence when BSA-FITC and BSA were injected every 100 s over 3.3 h, for a total of 120 injections. After a transient regime of 2500 s, the intensity remains stable within 2% for at least 3 h, indicating that the injected volume is remarkably reproducible. The transient regime of 2500 s may appear long but it results from the injection period t_p = 100 s, yielding k_0 = 1.2 10^{-3} s^{-1}. It lasts the time needed to attain a constant concentration inside the reactor, starting from an arbitrary initial condition. It is equal to $3k_0^{-1}$, 2500 s in this experiment. This transient regime is identical for any open chemical reactor with a feeding rate k_0.

A key characteristic of a μCSTR is the range of the feeding rate k_0 that is experimentally accessible. The lower limit for the time between two injections, t_P, is the mixing time in the reactor τ_M , such that

$$max(k_0) = \frac{\beta}{\tau_M} \quad (3)$$

Table 1 Volume injected at each inlet, measured using a solution of 1 μM BSA-FITC mixed with unlabelled 100 μM BSA in 50 mM borate buffer pH 9.3. Errors correspond to one standard deviation

Inlet number	Injected volume (nL)
1	0.19 ± 0.01
2	0.16 ± 0.02
3	0.14 ± 0.01
4	0.15 ± 0.02

To measure τ_M in the μCSTR we acquired time-lapse images during the mixing phase using again BSA-FITC and BSA. Defining τ_M as the time needed to mix reagents to 99% completion, we obtained τ_M(BSA) = 7 s. As a result max(k_0) = 0.017 s^{-1} and min(t_P) = 7 s in our μCSTR (see ESI, Fig. S4†).

3.3 A pH oscillator in the μCSTR

To validate the μCSTR as an open microfluidic reactor capable of studying chemical reactions far from equilibrium we used the bromate-sulfite-ferrocyanide pH oscillator reported by Edblom and collaborators,[30] this we will call here the Edblom oscillator. In a macroscopic CSTR this system displays three different steady states depending on the feeding rate: low pH (<3.5), pH oscillations, and high pH (>5.5). Fig. 3 shows the time trace of the pH inside the μCSTR for the Edblom oscillator at different feeding rates for a typical experiment. The pH was measured using a pH-sensitive fluorescent dye (see Methods). In the μCSTR we also observe the three regimes: pH low, oscillations and pH high. In contrast to the macroscopic CSTR, and due to the digital character of the μCSTR, the injection events perturb the pH. The extent of this perturbation depends on the conditions. In Fig. 3, the states corresponding to pH low and high (t_p = 402 and 78 s, blue and black curves, respectively) are very weakly perturbed after an injection. The oscillatory state (t_p = 115 s, red curve) is more sensitive: the pH time trace clearly shows a sharp increase at every injection (Fig. 3B, arrows). The amplitude of this pH perturbation is periodic and reflects the intrinsic pH of the Edblom oscillator. When the oscillator is in the high pH phase, such as it happens at t = 800 s and 2200 s, for instance, injection of fresh reagents has no effect on the pH. However, when the oscillator is in its low pH phase, such as it appears at t = 1800 and 3200 s, for instance, the pH suddenly increases to 5.5 after one injection and stays constant for 100 s, before decreasing within 10 s to the intrinsic pH of the Edblom oscillator. This observation can be explained considering that the concentration of H^+ in the reactor changes upon two processes with distinct time scales. At short times, the pH changes due to the protonation equilibria of SO_3^{2-}, which are faster than 1 ms.[30] In our experimental conditions the injected reagents are clearly basic, such that, unless the pH inside the reactor is lower than 2, an injection results in a sharp increase of the pH. At longer times, the two core reactions of the Edblom oscillator come into action, producing and consuming H^+ at a significantly slower rate (10^2 s, Fig. 3B red trace)

$$BrO_3^- + 3HSO_3^- \rightarrow Br^- + 3H^+ + 3SO_4^{2-} \quad (4)$$

$$BrO_3^- + 4Fe(CN)_6^{4-} + 5H^+ \rightarrow HOBr + 4Fe(CN)_6^{3-} + 2H_2O \quad (5)$$

Interestingly, although one injection is capable of momentarily perturbing the pH, it does not affect the underlying chemical process responsible of the pH oscillations: indeed, the oscillation period is clearly distinct from the injection period (1500 s and 115 s, respectively, in this case). The fact that the pH oscillator is resilient to the perturbations introduced by the injection process indicates that it is a limit cycle-type oscillator. By definition, the system returns to the limit cycle after any small perturbation from the closed trajectory.[10] This question will be discussed below (Fig. 6).

In a closed reactor, the dynamic behaviour of a chemical system depends both on the rate constants of the different chemical reactions and on the initial concentrations of the reactants. In a CSTR, k_0 and the input concentrations are

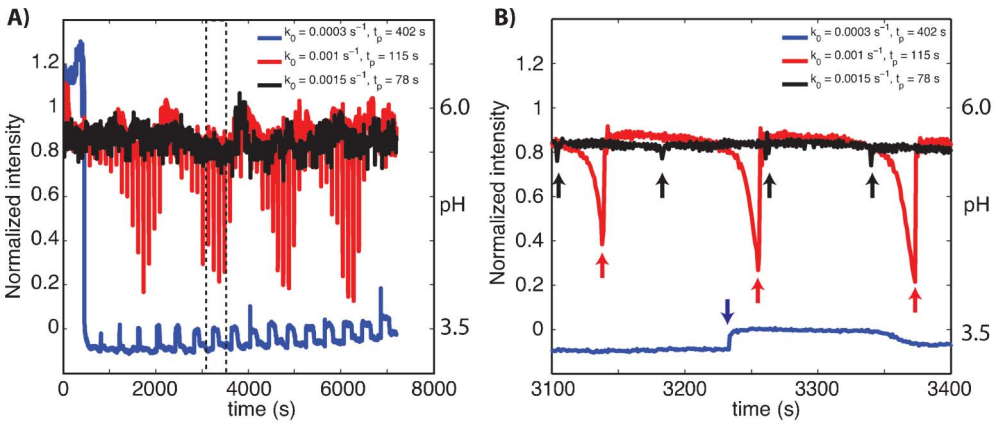

Fig. 3 The three states of the Edblom oscillator inside the μCSTR at constant input concentration. Normalized average fluorescence intensity and corresponding pH for different injection periods, t_p, and their corresponding feeding rates, k_0. Low pH (blue, t_p = 402 s), oscillations (red, t_p = 115 s) and high pH (black, t_p = 78 s). Input solutions were 20 mM $K_4[Fe(CN)_6]$, 65 mM $KBrO_3$, 75 mM Na_2SO_3, and 5 mM H_2SO_4. Panel B shows a temporal zoom of the dotted area in panel A. The arrows indicate the injection events.

additional parameters that can be easily tuned, offering a set of control knobs to explore chemical dynamics far from equilibrium. The values of the rate constants being fixed, the dynamic behaviour of the Edblom oscillator may be displayed in a five-dimensional phase-space: k_0, $[K_4Fe(CN)_6]^{IN}$, $[KBrO_3]^{IN}$, $[Na_2SO_3]^{IN}$, $[H_2SO_4]^{IN}$. Fig. 4 top shows the experimental phase diagram of the Edblom oscillator in the μCSTR along k_0 and $[Na_2SO_3]^{IN}$. The diagram is coded such that the colour of the curve inside each square corresponds to the nature of the dynamic state that is stable for a pair k_0 -$[Na_2SO_3]^{IN}$: blue for low pH, green for forced oscillations, red for sustained oscillations, and black for high pH. Within each square appears the actual pH time series for a 2 h period. The diagram is very similar to the one reported for the macroscopic CSTR.[30] At low $[Na_2SO_3]^{IN}$ the oscillator remains in the low pH steady state (blue curves), even at high values of k_0. At high values of $[Na_2SO_3]^{IN}$ four regimes are observed. At low and high values of k_0, low and high pH are, respectively, the stable states. At intermediate values of k_0 two distinct oscillatory behaviours appear: forced oscillations locked on the injection period (green curves) and sustained oscillations with a period significantly longer than the injection period (red traces). The period of the sustained oscillations spans from 600 to 1500 s, which is 10 times longer than the injection period, indicating that these two processes are distinct. In the macroscopic CSTR forced oscillations were not observed because the volume of one injection is infinitesimal. In the μCSTR presented here, each injection refreshes the contents of the reactor by 12% and thus introduces a perturbation in the chemical system that is not negligible. However, we see that for the pH oscillator studied here the perturbation due to the digital injection does not fundamentally change its behaviour. Importantly, the μCSTR strongly reduces the amount of sample consumed, 10^6-fold lower than for a typical 10 mL CSTR. The smallest CSTR so far reported has a volume of 0.1 mL and was used to set up a feedback-controlled enzymatic pH oscillator.[31] The authors clearly stated that the large consumption of their CSTR was an issue: up to 2 g of enzyme were needed to record a full phase diagram. Our μCSTR opens the way to study enzymatic reactions with low reagent consumption.

3.4. Simulations

Edblom and colleagues proposed a mechanism involving 9 reactions (see ESI†) that was sufficient to reproduce the three

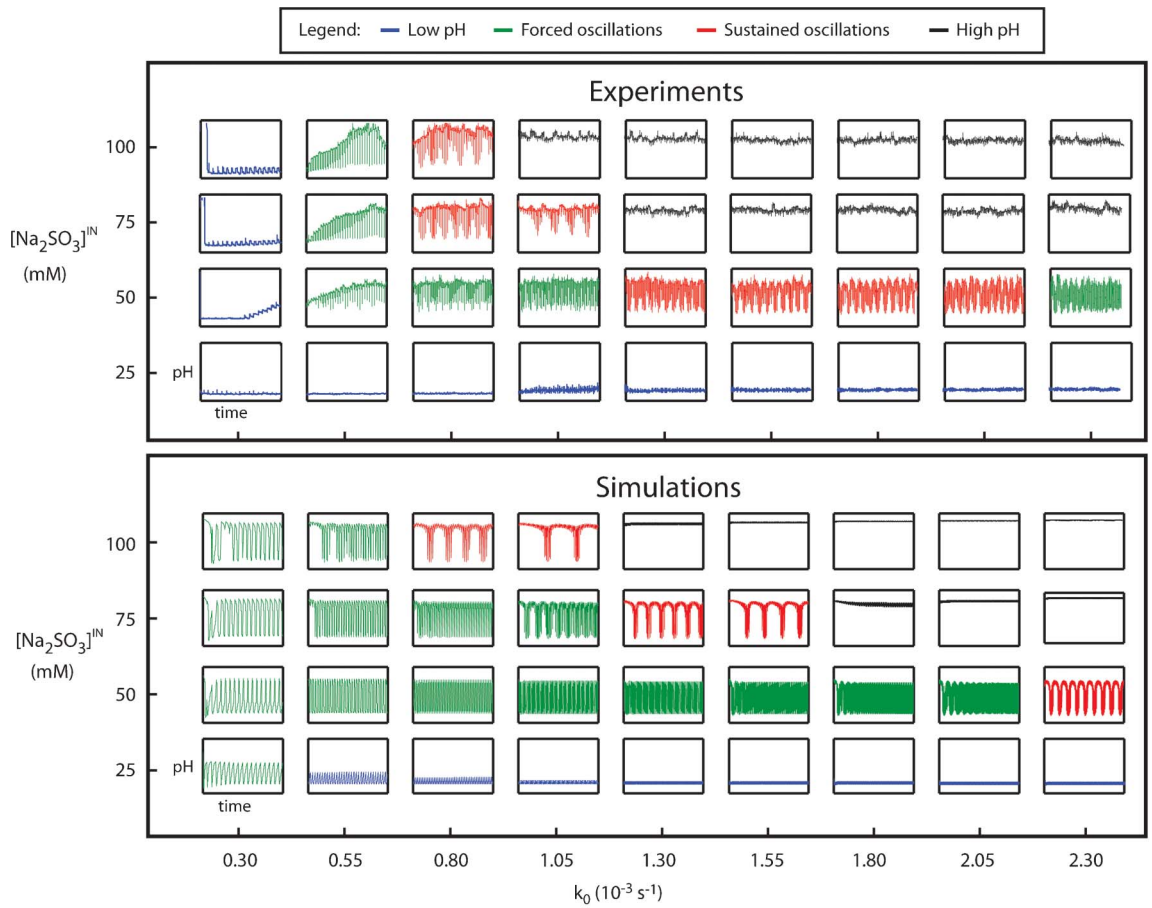

Fig. 4 Experimental (top) and simulated (bottom) phase diagram of the Edblom oscillator in the μCSTR for different Na_2SO_3 input concentrations and at different feeding rates k_0. Each square represents pH *vs.* time during a 2 h experiment. Time traces are colour-coded according to the observed steady state: low pH (blue), forced oscillations (green), sustained oscillations (red), and high pH (black). These are enlarged and shown in the supplementary materials. In the experiments $[H_2SO_4]$ = 5 mM while in the simulations $[H_2SO_4]$ = 10 mM. The remaining injected concentrations are $K_4[Fe(CN)_6]$ 20 mM and $KBrO_3$ 65 mM.

observed steady-states of their oscillator in a CSTR.[30] This mechanism, when solved numerically, was in semi-quantitative agreement with their experimentally measured phase diagram. To assess the differences between the macrofluidic and the microfluidic implementation of a CSTR on the Edblom oscillator, we implemented a numerical simulation of the same mechanism in the μCSTR. Two open questions were the influence of the digital injection and mixing, as well as the effect of the miniaturization of the reactor, notably the possible loss of Br_2, which is an important intermediate in the mechanism, through the porous walls of PDMS. To account for the digital injections we used an approach proposed by Farfel and Stefanovic, who were the first to discuss a theoretical implementation of a μCSTR.[32] For each species i eqn (1) was rewritten as

$$\frac{dC_i(t)}{dt} = (1-H)f_i\left(k_j, C_l(t)\right) + H\frac{k_0}{t_{\text{inj}}}\left(C_i^{\text{IN}} - C_i(t)\right) \qquad (6)$$

where H is a function that takes into account the digital character of the injection. It is equal to 1 during the injection phase, that lasted t_{inj} = 5 s in our simulations, and equal to 0 otherwise. Note that this implementation assumes perfect mixing as soon as the injection phase ends (see ESI, section 6.1†, for further discussion).

The experimental and simulated phase diagram of the Edblom oscillator in the same conditions (5 mM H_2SO_4, 20 mM $K_4[Fe(CN)_6]$, and 65 mM $KBrO_3$), displayed in Fig. S11†, are significantly different. Several reasons can be invoked to explain this discrepancy: (i) mixing in the experiments takes 7 s, while in the simulations it is instantaneous, (ii) injection and mixing are considered independent processes in the simulations, but they are simultaneous, and coupled to spatial transport, in the experiments, (iii) the high surface to volume ratio of the CSTR is not taken into account in the simulations, notably the evaporation of important intermediates such as Br_2 through the porous walls of PDMS, and (iv) the influence of the fluorescent dye is disregarded in the simulations. Instead of studying each of these processes in detail we decided to take a phenomenological description. To do so we performed a series of experiments, and the corresponding simulations, for different concentrations of H_2SO_4 and Na_2SO_3 using the CSTR as a closed reactor. In these experiments the four reagents were injected 50 consecutive times into the annular reactor and mixed to create a reproducible initial condition corresponding to 1/4 of the volume of the reactor for each injected solution. Subsequently, the injection valves were closed, mixing remained active, and fluorescence was recorded. The results are displayed in Fig. 5. For all the experiments the fluorescence intensity (the pH) stays high and stable until it abruptly drops and remains low. The time at which the fluorescence (pH) drops depends on $[Na_2SO_3]$ and $[H_2SO_4]$. The behavior of the Edblom oscillator at 5 mM H_2SO_4 in a closed reactor is significantly different for the experiments and the simulations. In contrast, results are similar when we compare simulations and experiments at 5 and 10 mM H_2SO_4 respectively. We argue that increasing the concentration of H_2SO_4 in the simulations to 10 mM phenomenologically takes into account the factors evoked above which are not incorporated in the simulations. We thus compare, in Fig. 4, the experimental phase diagram at 5 mM H_2SO_4 with the simulated phase diagram at 10 mM H_2SO_4. Overall, this small correction allows to compute individual pH time traces and a phase diagram that are in semi-quantitative agreement to those obtained experimentally.

Fig. 4 bottom displays the simulated phase diagram of the Edblom oscillator in the same conditions as the experimental phase diagram in Fig. 4 top, except that $[H_2SO_4]_{\text{sim}}^{\text{IN}}$ = 10 mM in the simulations while $[H_2SO_4]_{\text{exp}}^{\text{IN}}$ = 5 mM in the experiment. The four observed behaviours: low pH, forced oscillations, sustained oscillations and high pH, are captured by the simulations. Oscillations and high pH states are observed at comparable values of $[Na_2SO_3]^{\text{IN}}$ and k_0, both in experiments and simulations. Low pH state is dominant at low $[Na_2SO_3]^{\text{IN}}$ in both cases. There is only one feature that this model is not able to reproduce: low pH state is observed for all values of $[Na_2SO_3]^{\text{IN}}$ at low k_0 in the experiments while in the simulations forced oscillations dominate. This disagreement is intrinsic to the model proposed by Edblom *et al.*[30] When the four reagents of the Edblom oscillator are mixed in a closed reactor, the evolution of the pH over time is sigmoidal: an initial plateau at high pH is followed, within 20 to 400 s, by a sharp drop to low pH that is the final state of the reaction (Fig. 5). The model does not perfectly match this behaviour: the plateau and the sharp drop are quantitatively reproduced but, after 100 s at low pH, the pH increases strongly and remains high. This disagreement implies that, for the lowest value of k_0 in our μCSTR, corresponding to an injection period

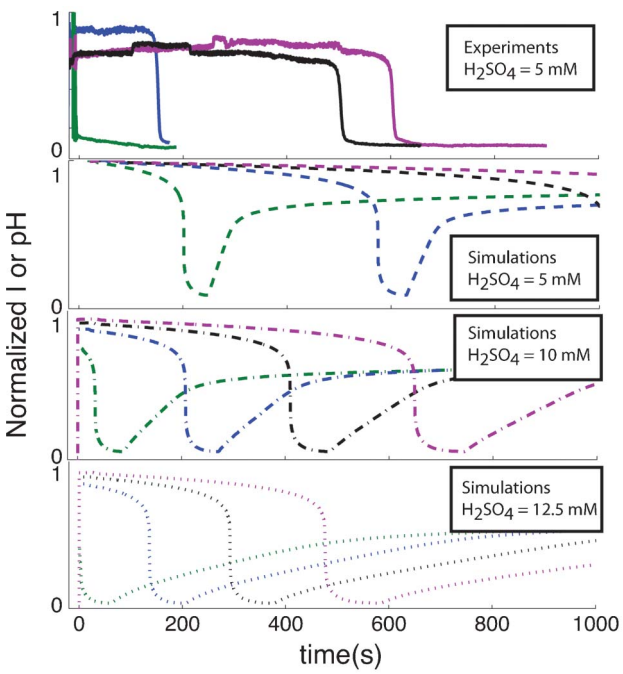

Fig. 5 Normalized intensity (experiments, solid lines) or normalized pH (simulations, dashed and dotted lines) *vs.* time after mixing in a closed reactor for different initial concentrations of Na_2SO_3 (25 mM, green, 50 mM, blue, 75 mM, black, and 100 mM, magenta) and H_2SO_4. The remaining initial concentrations were 20 mM $K_4[Fe(CN)_6]$ and 65 mM $KBrO_3$.

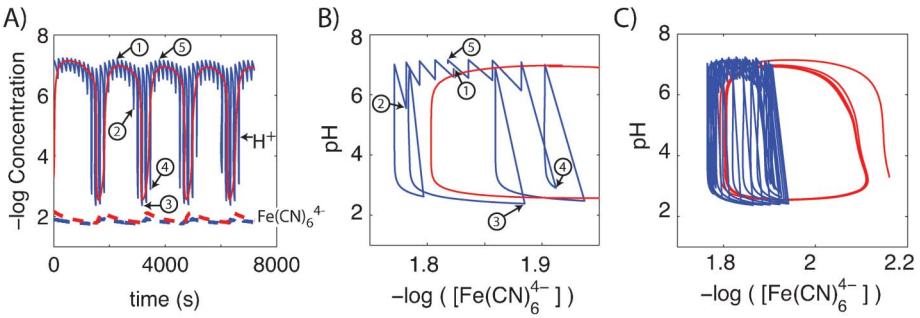

Fig. 6 The pH oscillator in the μCSTR is a limit cycle. All graphs show simulations for a digital CSTR, in blue, and a continuous CSTR, in red, for the same conditions. (A) Time series for $[H^+]$, solid line, and $[Fe(CN)_6^{4-}]$, dashed line. (B) Phase portrait of the data in panel A projected on $[H^+]$ and $[Fe(CN)_6^{4-}]$ for one period (t = 2350 − 3990 s). Numbers with arrows correspond to identical points in panels A and B. (C) Same as B for t = 0–7200 s. $k_0 = 8\ 10^{-3}\ s^{-1}$, input solutions were 20 mM $K_4[Fe(CN)_6]$, 65 mM $KBrO_3$, 100 mM Na_2SO_3, and 10 mM H_2SO_4.

of 402 s, the simulated pH will always return to the high state after every injection, as displayed in Fig. 4B. The code for the simulations is available in the ESI†.

We finish by discussing why the digital injection in the μCSTR momentarily perturbs the pH but does not preclude oscillations. Fig. 6 compares simulations of the Edblom oscillator for a digital CSTR, such as the μCSTR, and for a continuous one, where every injection of fresh reagents is infinitesimal. They correspond to the same conditions of k_0 and C_i^{IN}. The oscillation period is identical in both cases, as well as the amplitude of pH oscillations. The amplitude of $[Fe(CN)_6^{4-}]$ oscillations is reduced by half in the digital case. When the same data are displayed as a phase portrait in the $[H^+]$–$[Fe(CN)_6^{4-}]$ plane, Fig. 6B and C, it appears clear that the pH oscillator remains a limit cycle-type oscillator in the digital CSTR. In the phase portrait the variation in the concentrations during an injection is represented with an oblique straight line in the southeast-northwest direction. During the phase of the oscillator corresponding to high pH the injection of basic reagents has a small influence in the pH, and we observe a saw-teeth trajectory. During the phase corresponding to low pH the injection of basic reagents has a strong influence in the pH: during injection the pH switches to high followed by a pH drop at constant $[Fe(CN)_6^{4-}]$, then a $[Fe(CN)_6^{4-}]$ drop at constant pH. An injection will only switch the state of the oscillator from low to high, or *vice versa*, when it happens on the left or right side of the limit cycle (points 2 and 4 in Fig. 6A and B). The limit cycle in the digital CSTR corresponds to the contour of the blue trajectory in Fig. 6C.

4. Conclusion

We have shown that the well-known microfluidic rotary pump can be used as a micro continuous stirred tank reactor (μCSTR) for studying chemical systems far from equilibrium, such as a pH oscillator. The μCSTR presented here has a volume of 5.2 nL, 10^6-fold smaller than typical CSTRs and 10^4-fold smaller than the smallest reported CSTR.[31] The range of feeding rates covered was $k_0 = 0.3 - 2.3\ 10^{-3}\ s^{-1}$, where the upper boundary was limited by the mixing time, 7 s in our case. We used fluorescence to measure the concentration of protons. However, the μCSTR is compatible with other detection strategies such as electrochemical,[33] plasmon resonance, or nanotube impedance sensors.[34] The low volume and the range of k_0 reported here are particularly well suited for studying the dynamics of two recently engineered oscillators based on DNA and enzymes,[14,15] with typical oscillation periods of 100 min. We anticipate that our μCSTR will also be advantageous for observing complex dynamic behaviours in strand-displacement DNA cascades, with which the implementation of highly complex logical operations has been demonstrated experimentally[35–37] but the generation of oscillations, chaos and other dynamically interesting behaviours has only been shown theoretically.[38] Finally, it would be interesting to investigate biochemical processes that, when performed in a closed reactor, are limited by the consumption of energised reagents, such as it happens for transcription and protein expression with NTPs.

5. Materials and methods

5.1. Chemicals

Fluorescein, BSA, BSA-FITC, $K_4[Fe(CN)_6]\cdot 3H_2O$, H_2SO_4, $KBrO_4$, Na_2SO_3 were purchased from Sigma-Aldrich. 2′-7′-Difluorofluorescein (Oregon Green) came from Invitrogen. PDMS prepolymer RTV-615 kit was from GE. SU8 2050 and AZ9260 photoresist from Microchem and AZ Electronic Materials, respectively. Solutions were prepared with 1 MOhm deionized water. H_2SO_4 and $KBrO_4$ stock solutions at 100 and 260 mM, respectively, were stored for 1 month at room temperature. $K_4[Fe(CN)_6]$ and Na_2SO_3 solutions were discarded after two days. All working solutions were filtered through 1 μm cellulose filters (Minisart, Sartorius Stedim) and stored in 500 μL aliquots ready to use. Prior to each experiment Oregon Green was added to the input solutions at 10 μM final concentration.

5.2. Device fabrication and operation

Our micro-devices were fabricated in polydimethysiloxane using multilayer soft lithography.[25] Briefly, moulds were fabricated by photolithography with 10 μm thick AZ9260 and 50 μm thick SU8 2050 resist for flow and control channels, respectively. The photoresist of the flow channel mould was reflowed at 160 °C for 10 min to create rounded channels. The flow channel PDMS bottom layer was obtained by spin coating the PDMS mixture (ratio cross-linker/monomer = 1 : 20 w/w) at 1900 rpm for 60 s on the corresponding mould. During that time, a 5 mm-thick, 1 : 5 w/w PDMS mixture was cast on the control channel mould. Both PDMS layers were partially cured at 70 °C for 45 min. Then, the thick PDMS layer was peeled off from its mould, visually aligned under a binocular microscope and placed on the thinner one. After bonding at 70 °C for 45 min, the monolithic PDMS structure was peeled off, the inlets were punched, and the device was bonded on the substrate. We worked both with a PDMS flat layer or a glass slide as substrates. Bonding was either reversible, using thermal bonding of partially cured PDMS, or irreversible, using air-plasma surface activation (Plasma Cleaner, Harrick Plasma).

Each valve functions by applying pressure to a control channel (situated on the upper PDMS layer) to deform the membrane at the cross area between the control and the flow channel, which closes the later. Since PDMS is permeable to gases, the control channels were filled with water to avoid bubble formation in the flow channels during valve operation.

The injection and mixing pumps are made of three in-line valves, allowing peristaltic pumping. The three valves of the mixing pump were actuated with a 001 101 100 110 111 pattern (1 close, 0 open, a complete pumping cycle is performed in 50 × 5 = 250 ms, *i.e.* 4 Hz). The fastest mixing, characterized by fluorescence imaging, occurred in 7 s with a control channel pressure of 500 mbar. The three valves of the injection pump were actuated following the same pattern, which is executed once for one injection. Note that at least one valve remained always closed, such that injection is independent of the inlet pressure and successive injections are highly reproducible. In between two injection events, the mixing pump was actuated and the injection valve 1 was closed such that the reactor was isolated from the inlets and the outlet. Injection valves 2 and 3 remained open to allow the renewal of reactants in the inlets through the dedicated purge channel. In the absence of this purge the pH of the bromate solution inside the PDMS channel is not stable (ESI, Fig. S6†).

The pressure controller was commanded through Matlab (The MathWorks). The pressure inside the control channels responsible of valve actuation was switched on and off *via* a home-made controller including an Arduino Duemilanove USB DAQ and a set of solenoid microvalves from LeeCorp. The input pressure was manually set with a pressure regulator (8601, Brooks) and a digital gauge with 1 mbar precision (LEO 2, Keller). All air tubing connexions were set using Tygon tubes 1/8 or 1/16″ ID and luer connectors. Sample reservoirs connected to the chip were fabricated using a short portion of a 1/8″ ID Tygon tube connected to a Microline tube (1.5 mm OD, 0.6 mm ID and 5 cm long) and to a stainless steel connector (0.025″ OD, 0.016″ ID, New England Small Tube Corp.) that fitted into the chip inlets.

5.3. Image acquisition and μCSTR experiments

Fluorescence images were acquired with either an Olympus IX71 microscope with an Orca R2 Hamamatsu CCD camera carrying a GFP BrightLine filterset (excitation 472/30, dichroic 295, emission 520/35, Semrock) or a Zeiss Axio Observer Z1 microscope equipped with a Hamamatsu C9100 CCD camera and a Zeiss 38 HE eGFP filterset (EX BP 470/40, BS FT 495, EM BP 525/50). In both cases a 2.5 X, N.A. 0.075 objective from Zeiss was employed. Typical exposure time was 100 ms and binning was set to 2, yielding a 10 S/N per pixel. For time-lapse experiments, an image was recorded every 1 or 10 s. To reduce photobleaching we used an automatic shutter, such that the sample was exposed to the excitation light less than 200 ms at each image capture. As a result, bleaching was smaller than 5% during the experiments with the longest interval between two injections being t_p = 402 s. Image acquisition and analysis was performed using Micro-Manager 1.4 (open source microscopy software[39]).

A μCSTR device was controlled with five different pressure sources. The control channels for the injection pump, with a PDMS membrane cross-section of 100 × 100 μm^2, were set to 1500 mbar; the control channels for the mixing pump, with a PDMS membrane cross-section of 200 × 200 μm^2, were set to 500 mbar; the inlet channels carrying fresh reagents were pushed at 150 mbar; and purge channels were kept at 120 mbar. The outlet channel was kept at 50 mbar to maintain the whole device slightly above atmospheric pressure and avoid bubbles. The pH inside the chip was monitored using a pH-dependent fluorophore, Oregon Green, at 10 μM. The fluorescence intensity *vs.* pH response of the fluorophore was linear in the range 3.75–6 provided that the concentrations of $K_4[Fe(CN)_6]$ and Na_2SO_3 inside the reactor were below 50 and 200 mM, respectively (see ESI, Fig. S1, S2†). The fluorescence intensity inside the reactor was averaged over a 100 × 200 pixel area to yield I_{raw}. A normalized intensity was computed $I_{norm} = (I_{raw} - I_{acid})/(I_{sulfite} - I_{acid})$, where I_{acid} and $I_{sulfite}$ are the intensities recorded in the sulfuric acid and sodium sulfite inlets, respectively. A typical μCSTR experiment was performed overnight, scanning 9 different injection periods sequentially from 402 to 52 s. For each injection period the fluorescence was recorded during 2 h. The initial conditions of run $n + 1$ corresponded to the final conditions of run n. The concentrations of the injected solutions are given inside the reactor, their concentrations inside the inlet channels are thus four times larger.

Acknowledgements

This research was supported by a grant from Triangle de la physique under award Microgradients. We thank P. de Kepper for advice, C. Gosse for kindly giving us access to a fluorescence microscope, G. Morel for analysis, and I. el Abdouni and J. Dias for performing preliminary experiments.

References

1 K. R. Mitchelson, *New high throughput technologies for DNA sequencing and genomics*, Elsevier, Amsterdam, 2007.
2 B. N. G. Giepmans, S. R. Adams, M. H. Ellisman and R. Y. Tsien, *Science*, 2006, **312**, 217–224.
3 R. Pepperkok and J. Ellenberg, *Nat. Rev. Mol. Cell Biol.*, 2006, **7**, 690–696.
4 A. Goldbeter, *Biochemical oscillators and biological rhythms*, *Cambridge University Press*, Cambridge, 1996.
5 J. J. Tyson, K. Chen and B. Novak, *Nat. Rev. Mol. Cell Biol.*, 2001, **2**, 908–916.
6 U. Alon, *An Introduction to Systems Biology: Design Principles of Biological Circuits*, CRC, Boca Raton, 2006.
7 U. Alon, *Nat. Rev. Genet.*, 2007, **8**, 450–461.
8 C. J. Kastrup, M. K. Runyon, E. M. Lucchetta, J. M. Price and R. F. Ismagilov, *Acc. Chem. Res.*, 2008, **41**, 549–558.
9 X. Chen and A. D. Ellington, *Curr. Opin. Biotechnol.*, 2010, **21**, 392–400.
10 I. Epstein and J. A. Pojman, *An introduction to nonlinear chemical reactions*, Oxford University Press, New York, 1998.
11 M. B. Elowitz and S. Leibler, *Nature*, 2000, **403**, 335–338.
12 N. Nandagopal and M. B. Elowitz, *Science*, 2011, **333**, 1244–1248.
13 B. Yurke, A. J. Turberfield, A. P. Mills, F. C. Simmel and J. L. Neumann, *Nature*, 2000, **406**, 605–608.
14 K. Montagne, R. Plasson, Y. Sakai, T. Fujii and Y. Rondelez, *Mol. Syst. Biol.*, 2011, **7**, 466.
15 J. Kim and E. Winfree, *Mol. Syst. Biol.*, 2011, **7**, 465.
16 M. Morel, J.-C. Galas, M. Dahan and V. Studer, *Lab Chip*, 2012, **12**, 1340–1346.
17 A. Estevez-Torres, T. Le Saux, C. Gosse, A. Lemarchand, A. Bourdoncle and L. Jullien, *Lab Chip*, 2008, **8**, 1205–1209.
18 B. T. Ginn, B. Steinbock, M. Kahveci and O. Steinbock, *J. Phys. Chem. A*, 2004, **108**, 1325–1332.
19 C. J. Kastrup, M. K. Runyon, F. Shen and R. F. Ismagilov, *Proc. Natl. Acad. Sci. U. S. A.*, 2006, **103**, 15747–15752.
20 M. K. Runyon, B. L. Johnson-Kerner, C. J. Kastrup, T. G. Van Ha and R. F. Ismagilov, *J. Am. Chem. Soc.*, 2007, **129**, 7014.
21 M. Toiya, V. Vanag and I. Epstein, *Angew. Chem., Int. Ed.*, 2008, **47**, 7753–7755.
22 M. Marek and E. Svobodov, *Biophys. Chem.*, 1975, **3**, 263–273.
23 P. De Kepper, I. R. Epstein and K. Kustin, *J. Am. Chem. Soc.*, 1981, **103**, 2133–2134.
24 I. R. Epstein, *J. Chem. Educ.*, 1989, **66**, 191–195.
25 M. A. Unger, H.-P. Chou, T. Thorsen, A. Scherer and S. R. Quake, *Science*, 2000, **288**, 113–116.
26 H.-P. Chou, M. A. Unger and S. R. Quake, *Biomed. Microdevices*, 2001, **3**, 323–330.
27 G. F. Froment and K. B. Bischoff, *Chemical reactor analysis and design*, Wiley, New York, 1990.
28 M. Takinoue, H. Onoe and S. Takeuchi, *Small*, 2010, **6**, 2374–2377.
29 F. Mugele and J. C. Baret, *J. Phys.: Condens. Matter*, 2005, **17**, R705.
30 E. C. Edblom, Y. Luo, M. Orban, K. Kustin and I. R. Epstein, *J. Phys. Chem.*, 1989, **93**, 2722–2727.
31 V. K. Vanag, D. G. Miguez and I. R. Epstein, *J. Chem. Phys.*, 2006, **125**, 194515.
32 J. Farfel and D. Stefanovic, *DNA computing 5, Lecture Notes in Computer Science*, Springer, Berlin, 2006, **3892**, 38-54.
33 F. Mavré, R. K. Anand, D. R. Laws, K.-F. Chow, B.-Y. Chang, J. A. Crooks and R. M. Crooks, *Anal. Chem.*, 2010, **82**, 8766–8774.
34 T. Kurkina, A. Vlandas, A. Ahmad, K. Kern and K. Balasubramanian, *Angew. Chem., Int. Ed.*, 2011, **50**, 3710–3714.
35 G. Seelig, D. Soloveichik, D. Y. Zhang and E. Winfree, *Science*, 2006, **314**, 1585–1588.
36 L. Qian, E. Winfree and J. Bruck, *Nature*, 2011, **475**, 368–372.
37 L. Qian and E. Winfree, *Science*, 2011, **332**, 1196–1201.
38 D. Soloveichik, G. Seelig and E. Winfree, *Proc. Natl. Acad. Sci. U. S. A.*, 2010, **107**, 5393–5398.
39 A. Edelstein, N. Amodaj, K. Hoover, R. Vale and N. Stuurman, *Computer Control of Microscopes Using μManager*, John Wiley & Sons, Inc., 2010.

Supplementary information for: A nanoliter-scale open chemical reactor

Jean-Christophe Galas, Anne-Marie Haghiri-Gosnet and André Estévez-Torres

Laboratoire de photonique et de nanostructures, CNRS,
route de Nozay, 91460 Marcoussis, France

October 15, 2012

Contents

1 Calibration of the *p*H inside the μCSTR

Figure 1 shows that the fluorescence of Oregon Green depends lineraly on *p*H in the range $3.7 - 6.0$. Figure 2 shows the effect of increasing concentration of the Edblom oscillator species on Oregon Green fluorescence. The presence of bromate has a negligible effect. In contrast, $NaSO_3$ and $K_4[Fe(CN)_6]$ clearly reduce the dye fluorescence at constant *p*H. The highest concentrations used in this work were $[NaSO_3] = 100$ mM and $[K_4[Fe(CN)_6]] = 65$ mM, resulting in a decrease of fluorescence of 20%, which was compatible with a correct determination of the *p*H inside the microreactor.

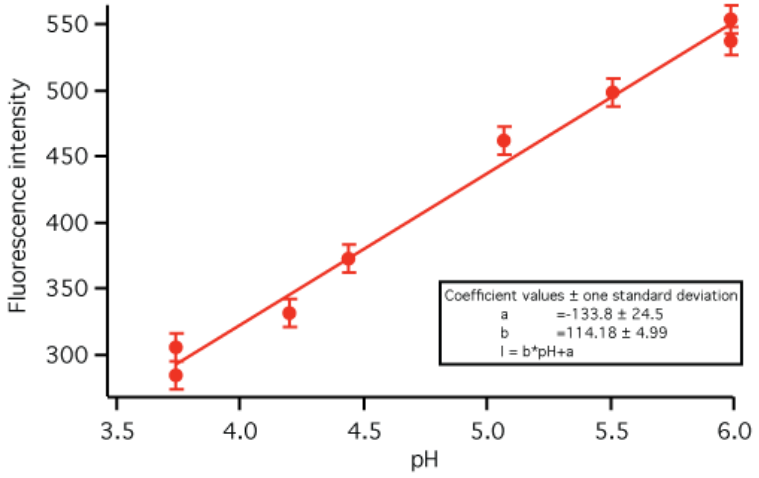

Figure S 1: Fluorescence intensity inside the μCSTR of a 10 μM solution of Oregon Green in buffers of different *p*H recorded with a 2.5X objective.

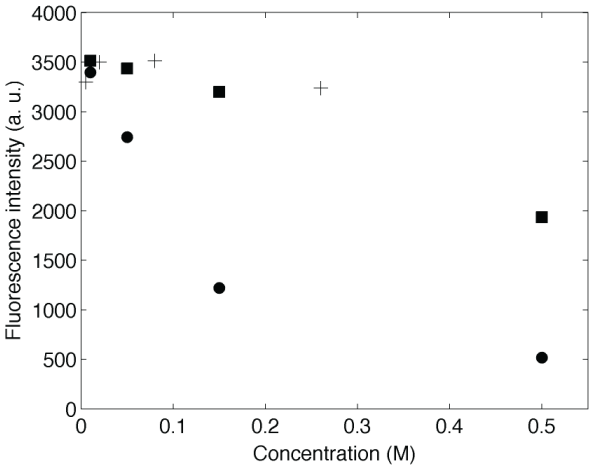

Figure S 2: Influence of reagent concentration on the maximum fluorescence intensity of Oregon Green 10 μM for $KBrO_3$ (crosses), $NaSO_3$ (squares), and $K_4[Fe(CN)_6]$ (disks).

2 3D view of the μCSTR

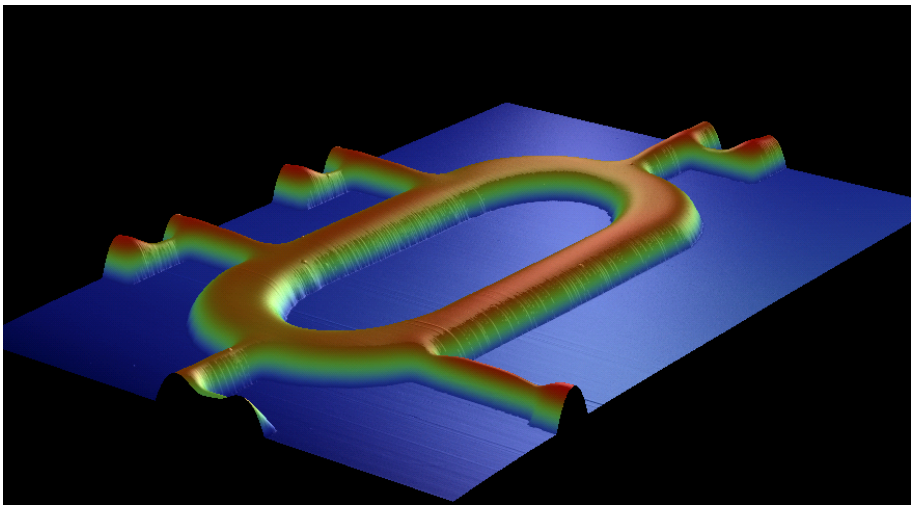

Figure S 3: 3D profile of the mould used to fabricate the μCSTR, acquired using a profilometer. The injection channels and the annular reactor are 100 and 200 μm wide, respectively. The height is color coded, the maximum height of the annular channel being 10 μm.

3 Reproducibility and influence of mixing

3.1 Determination of the mixing time

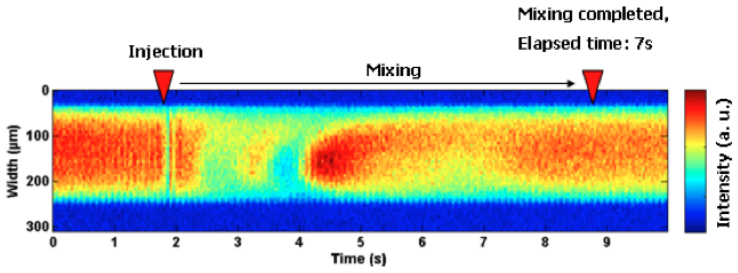

Figure S 4: Determination of the mixing time in the μCSTR. Fluorescent intensity profile across the width of the annular channel *vs* time (kymograph) during injection and mixing.

3.2 Influence of mixing on the behaviour of the Edblom oscillator in the μCSTR

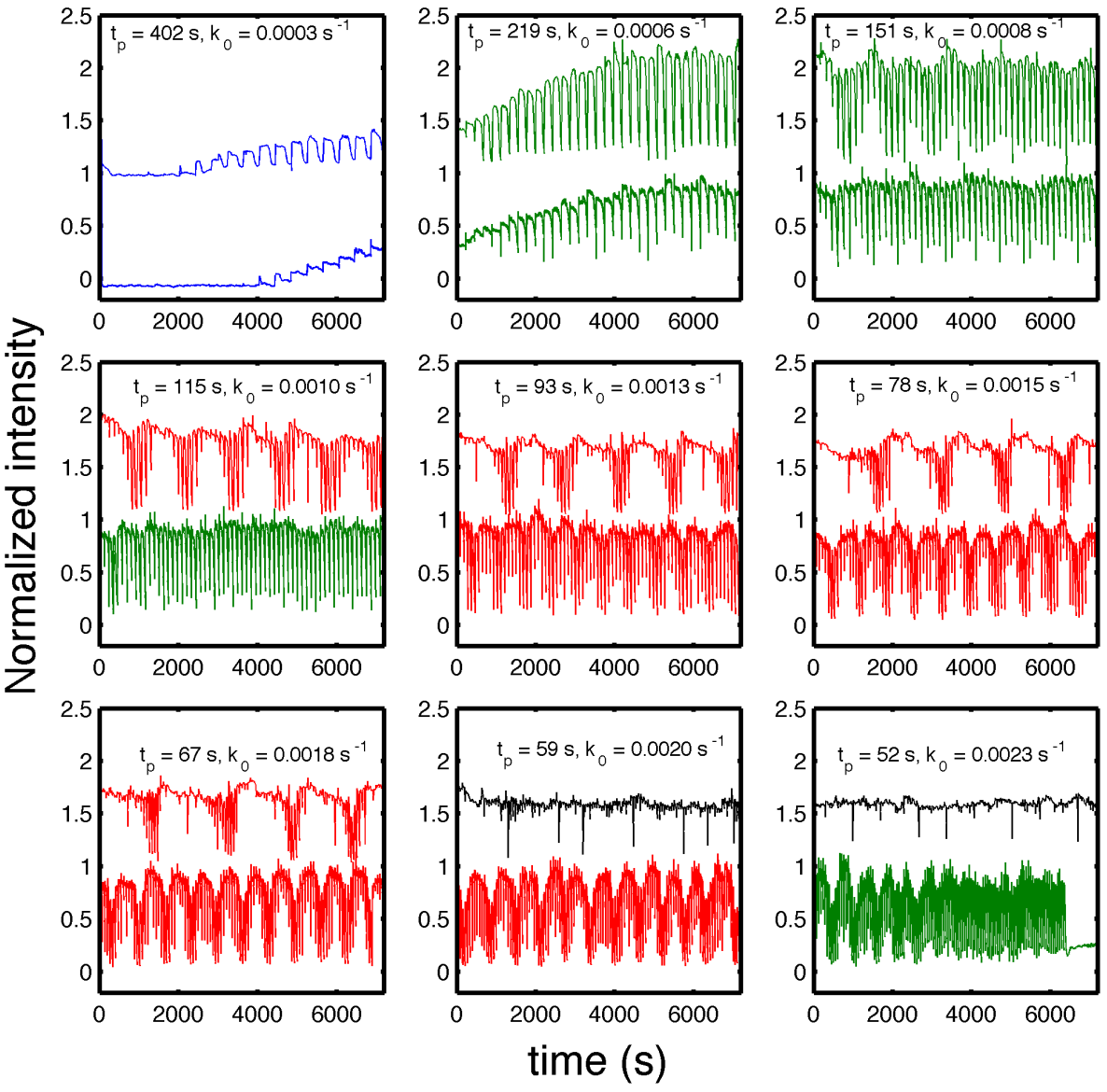

Figure S 5: Influence of mixing on the behavior of the Edblom oscillator. Normalized fluorescence intensities *vs* time for optimal mixing (lower curves) and non-optimal mixing (upper curves) at different injection periods, t_p, and their corresponding feeding rates, k_0. $[Na_2SO_3] = 50$ mM, $[H_2SO_4] = 5$ mM, $[\ K_4[Fe(CN)_6]\ ] = 20$ mM and $[KBrO_3] = 65$ mM. Optimal mixing was completed in 7 s, while non-optimal mixing took 20 s. Color indicates the state of the oscillator: low *p*H (blue), forced oscillations (green), sustained oscillations (red), and high *p*H (black). Curves are shifted vertically for clarity.

4 *p*H of the bromate channel with and without purging

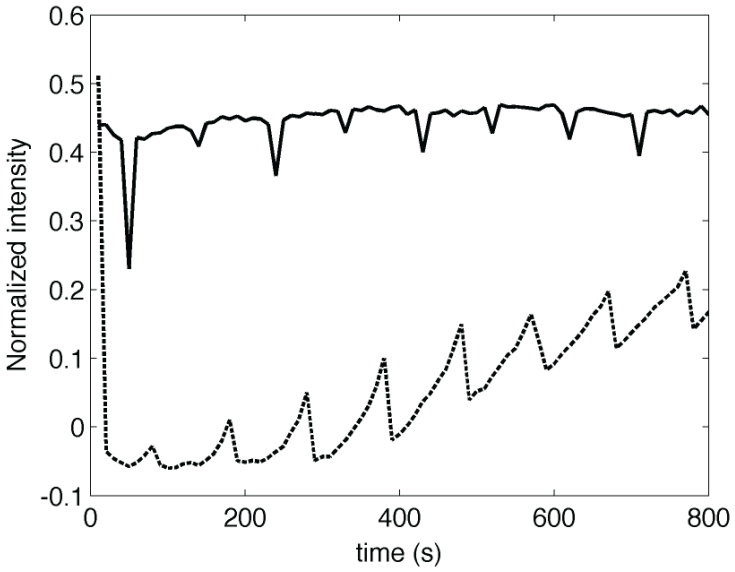

Figure S 6: Effect of the purging on the *p*H of the injected solution of $KBrO_3$ 65 mM. The *p*H is given by the fluorescence of Oregon Green 10 μM. Purging was on (solid line) or off (dashed line). The intensity was measured inside the injection channel, between valves 1 and 2.

5 Experimental *p*H *vs* time plots

In this section are displayed, in large format, the normalized fluorescence intensity *vs* time plots represented in the phase diagram in Fig. 5A in the Main Text. The following conditions are common to all graphs: 5 mM H_2SO_4, 20 mM $K_4[Fe(CN)_6]$, and 65 mM $KBrO_3$. The graphs are color-coded as in the Main Text: low *p*H (black), forced oscillations (green), sustained oscillations (red), and high *p*H (black).

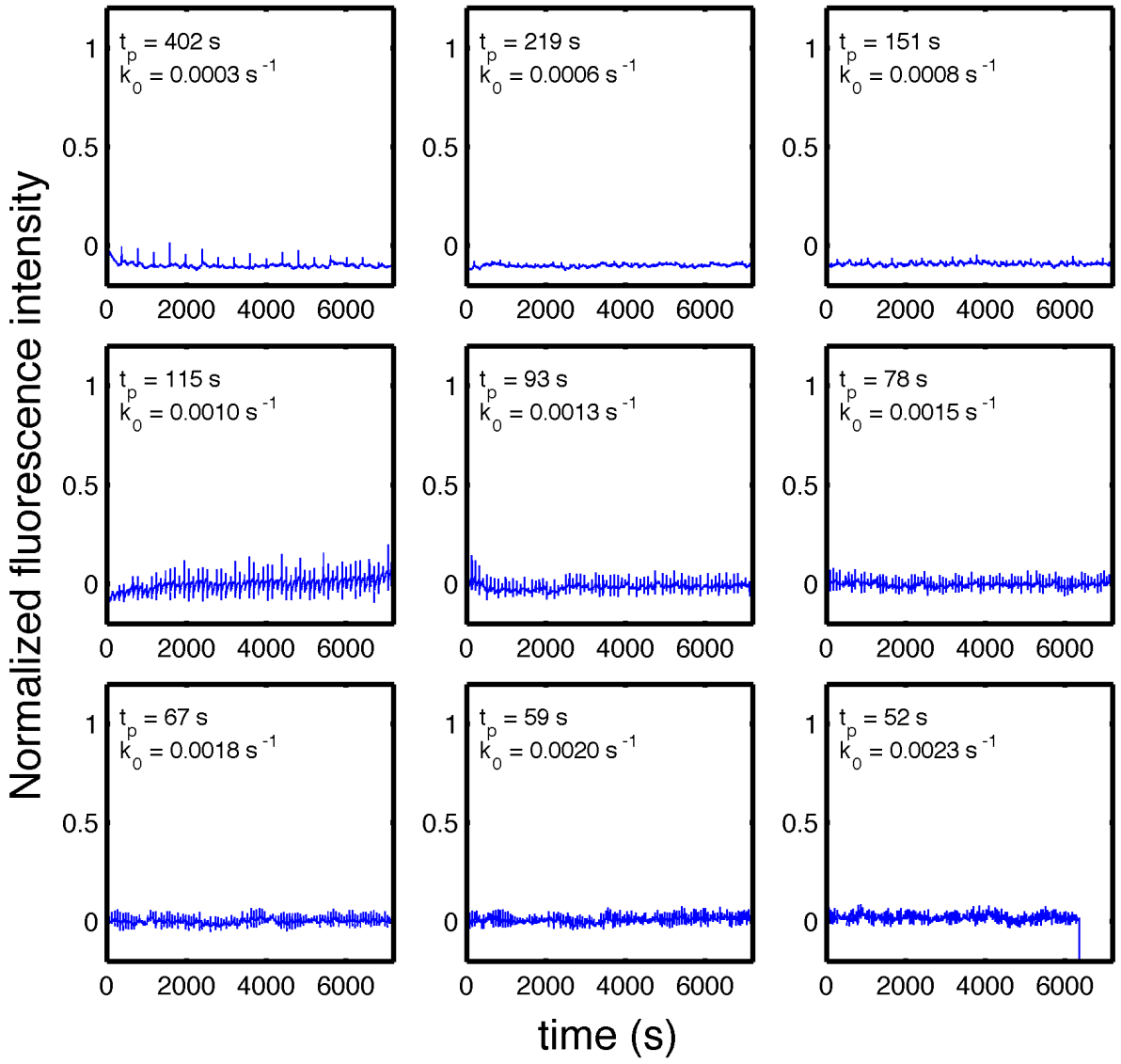

Figure S 7: Experimental normalized average fluorescence intensity for different injection periods, t_p, and their corresponding feeding rates, k_0, when the concentration of injected Na_2SO_3 was 25 mM.

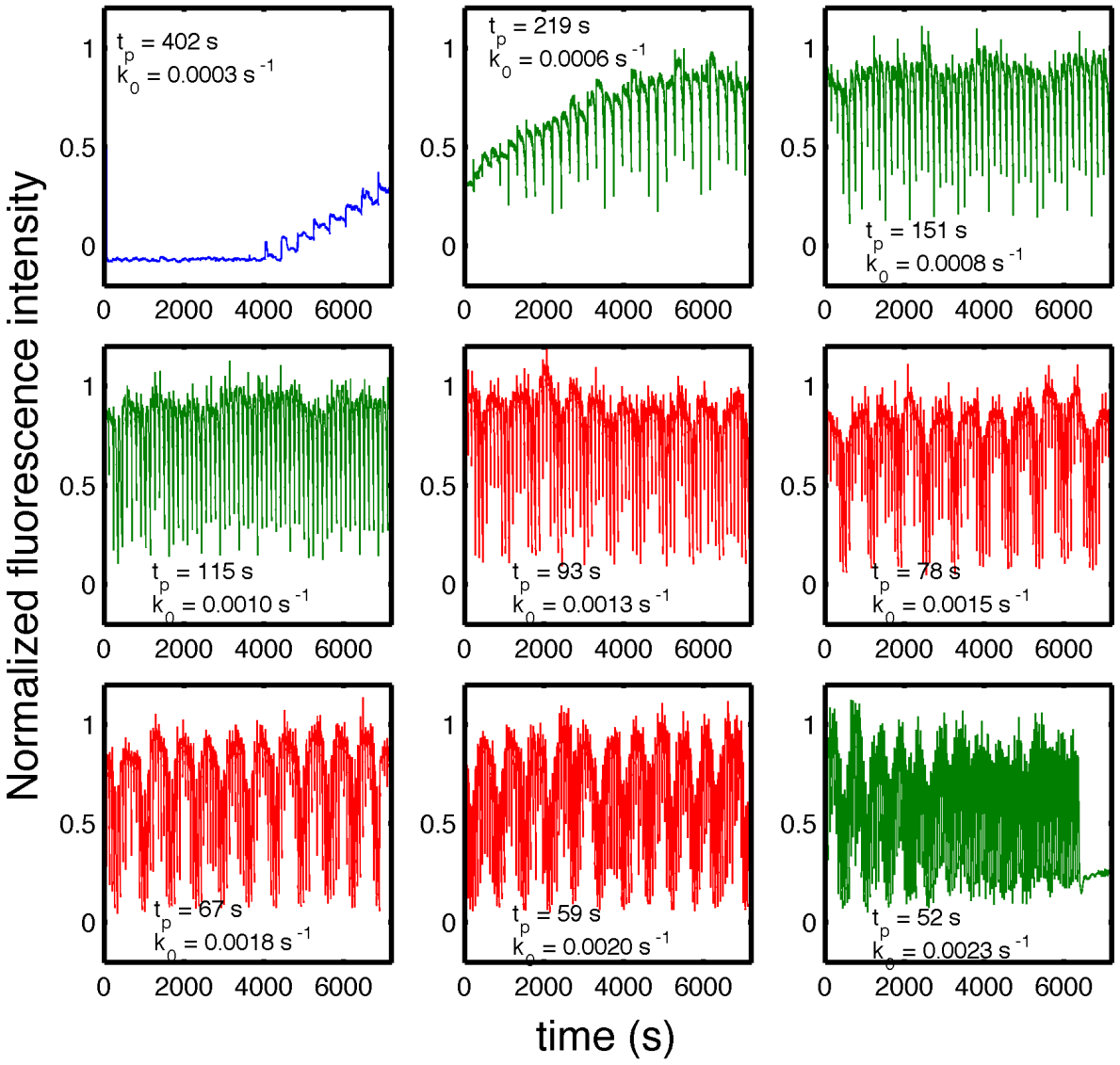

Figure S 8: Experimental normalized average fluorescence intensity for different injection periods, t_p, and their corresponding feeding rates, k_0, when the concentration of injected Na_2SO_3 was 50 mM.

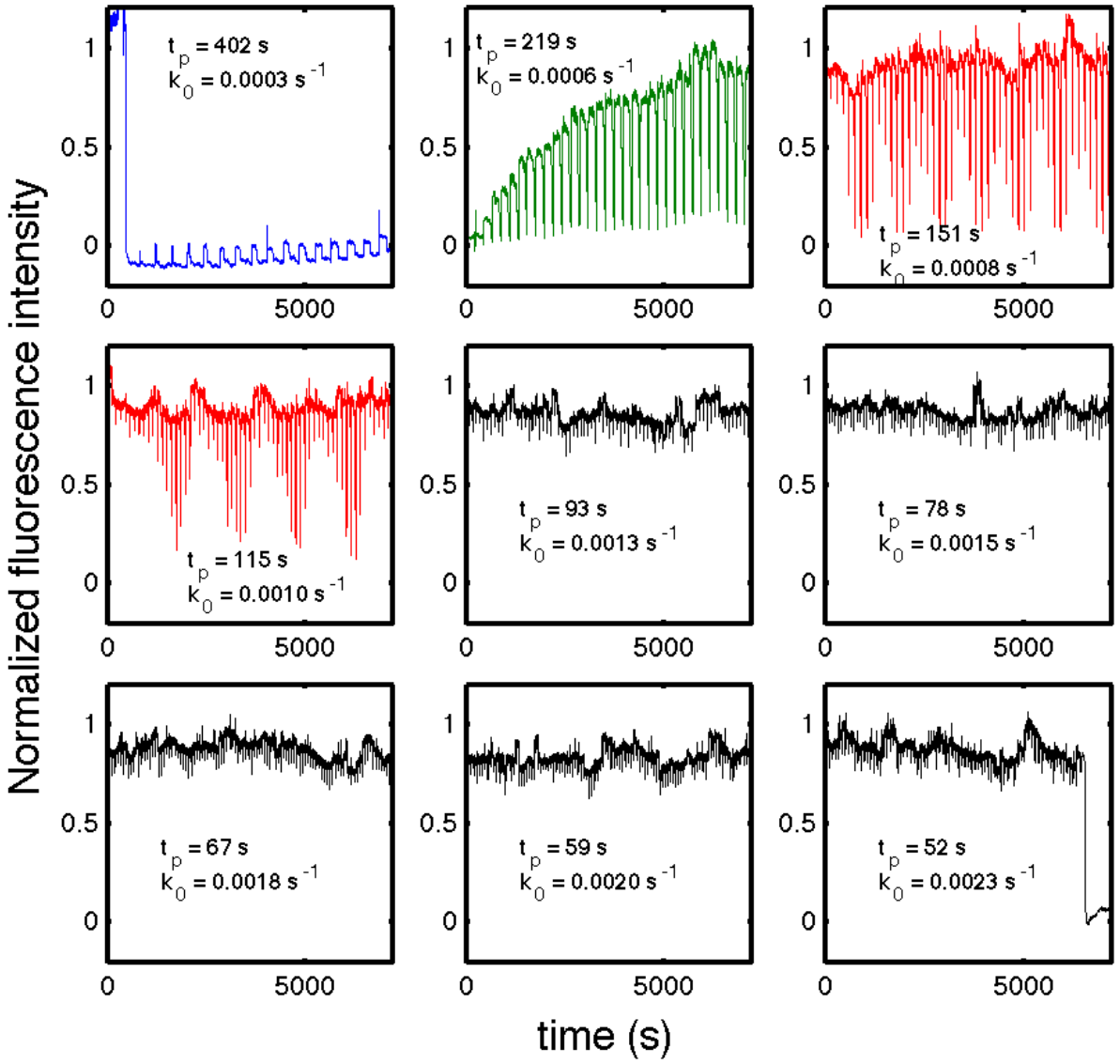

Figure S 9: Experimental normalized average fluorescence intensity for different injection periods, t_p, and their corresponding feeding rates, k_0, when the concentration of injected Na_2SO_3 was 75 mM.

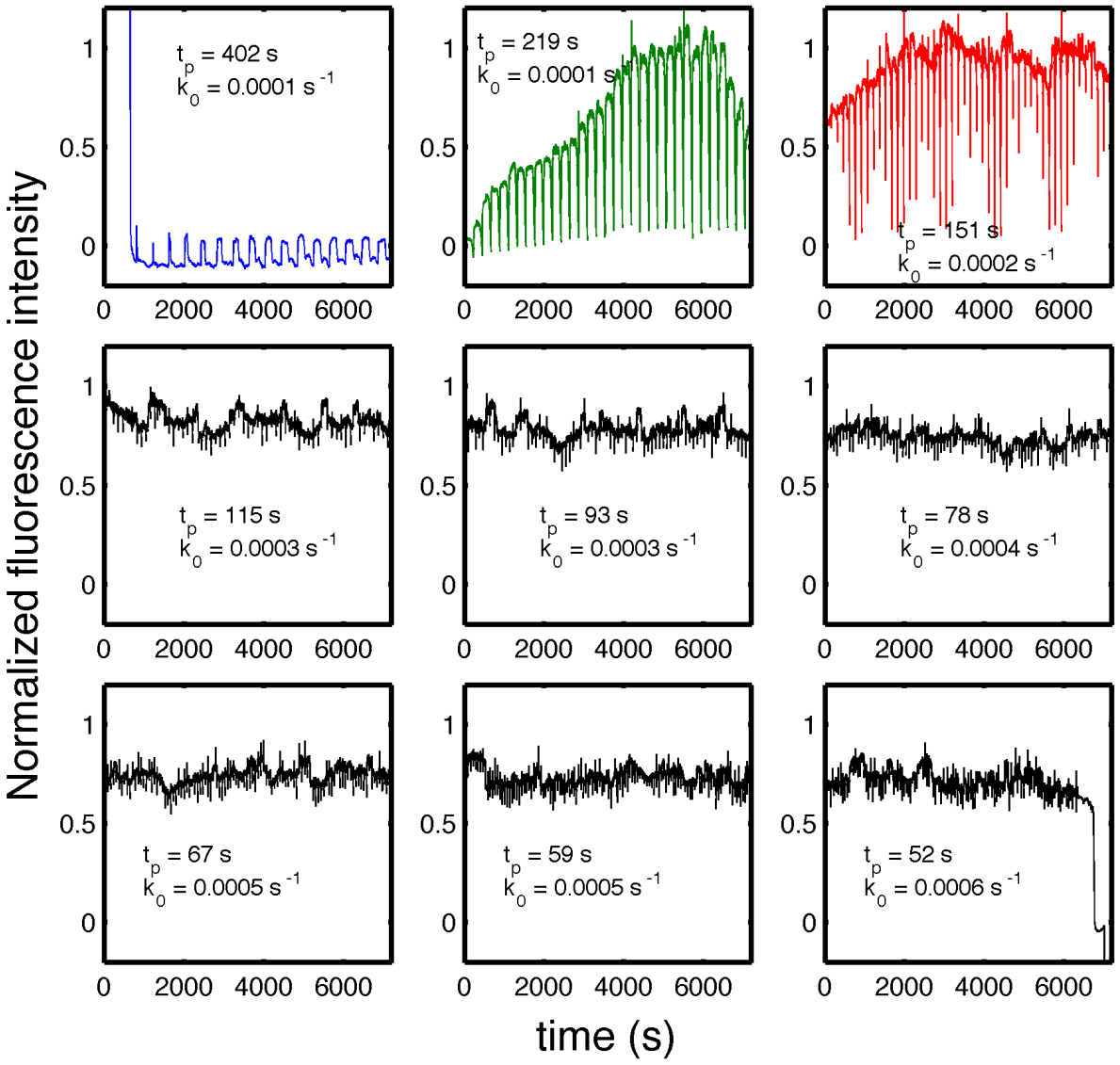

Figure S 10: Experimental normalized average fluorescence intensity for different injection periods, t_p, and their corresponding feeding rates, k_0, when the concentration of injected Na_2SO_3 was 100 mM.

6 Simulations

6.1 Model of the Edblom oscillator

Edblom et al[1] demonstrated that the main features of the oscillator studied in this work were described with the following set of reactions

$$\mathrm{BrO_3^- + HSO_3^-} \xrightarrow{k_1} \mathrm{HBrO_2 + SO_4^{2-}} \qquad k_1 = 8 \times 10^{-2}\mathrm{M^{-1}s^{-1}} \tag{1}$$

$$\mathrm{HBrO_2 + Br^- + H^+} \xrightarrow{k_2} \mathrm{2HOBr} \qquad k_2 = 9.5 \times 10^{6}\mathrm{M^{-2}s^{-1}} \tag{2}$$

$$\mathrm{HOBr + Br^- + H^+} \xrightarrow{k_3} \mathrm{Br_2 + H_2O} \qquad k_3 = 1.6 \times 10^{1}0\mathrm{M^{-2}s^{-1}} \tag{3}$$

$$\mathrm{Br_2 + H_2O} \xrightarrow{k_4} \mathrm{HOBr + Br^- + H^+} \qquad k_4 = 1.1 \times 10^{1}\mathrm{s^{-1}} \tag{4}$$

$$\mathrm{2HBrO_2} \xrightarrow{k_5} \mathrm{BrO_3^- + HOBr + H^+} \qquad k_5 = 3 \times 10^{3}\mathrm{M^{-1}s^{-1}} \tag{5}$$

$$\mathrm{Br_2 + HSO_3^- + H_2O} \xrightarrow{k_6} \mathrm{2Br^- + SO_4^{2-} + 3H^+} \qquad k_6 = 1.0 \times 10^{6}\mathrm{M^{-1}s^{-1}} \tag{6}$$

$$\mathrm{H^+ + SO_3^{2-}} \xrightarrow{k_7} \mathrm{HSO_3^-} \qquad k_7 = 5.0 \times 10^{10}\mathrm{M^{-1}s^{-1}} \tag{7}$$

$$\mathrm{HSO_3^-} \xrightarrow{k_8} \mathrm{H^+ + SO_3^{2-}} \qquad k_8 = 3 \times 10^{3}\mathrm{s^{-1}} \tag{8}$$

$$\mathrm{BrO_3^- + 2Fe(CN)_6^{4-} + 3H^+} = \mathrm{HBrO_2 + 2Fe(CN)_6^{3-} + H_2O} \tag{9}$$

$$\mathrm{BrO_3^- + Fe(CN)_6^{4-} + H^+} \xrightarrow{k_9} \mathrm{HBrO_2 + Fe(CN)_6^{3-} + H_2O} \qquad k_9 = 3.2 \times 10^{1}\mathrm{M^{-2}s^{-1}}, \tag{10}$$

where (9) defines the stœchiometry of the oxydation of $\mathrm{Fe(CN)_6^{4-}}$ and (10) accounts for the mechanism from which the rate is computed. The rates for reactions 1 to 9 are

$$r_1 = k_1[\mathrm{BrO_3^-}][\mathrm{HSO_3^-}] \tag{11}$$

$$r_2 = k_2[\mathrm{HBrO_2}][\mathrm{Br^-}][\mathrm{H^+}] \tag{12}$$

$$r_3 = k_3[\mathrm{HOBr}][\mathrm{Br^-}][\mathrm{H^+}] \tag{13}$$

$$r_4 = k_4[\mathrm{Br_2}] \tag{14}$$

$$r_5 = k_5[\mathrm{HBrO_2}]^2 \tag{15}$$

$$r_6 = k_6[\mathrm{Br_2}][\mathrm{HSO_3^-}] \tag{16}$$

$$r_7 = k_7[\mathrm{H^+}][\mathrm{SO_3^{2-}}] \tag{17}$$

$$r_8 = k_8[\mathrm{HSO_3^-}] \tag{18}$$

$$r_9 = k_9[\mathrm{BrO_3^-}][\mathrm{Fe(CN)_6^{4-}}][\mathrm{H^+}]. \tag{19}$$

The differential equations describing the temporal evolution of the species involved in the Edblom oscillator in a CSTR are thus

[1] E. C. Edblom, Y. Luo, M. Orban, K. Kustin and I. R. Epstein, *J. Phys. Chem.*, **1989**, 93, 2722-2727.

$$\frac{d[\mathrm{Br}^-]}{dt} = -r_2 - r_3 + r_4 + 2r_6 - k_0[\mathrm{Br}^-] \quad (20)$$

$$\frac{d[\mathrm{Br_2}]}{dt} = r_3 - r_4 - r_6 - k_0[\mathrm{Br_2}] \quad (21)$$

$$\frac{d[\mathrm{HOBr}]}{dt} = 2r_2 - r_3 + r_4 + r_5 - k_0[\mathrm{HOBr}] \quad (22)$$

$$\frac{d[\mathrm{HBrO_2}]}{dt} = r_1 - r_2 - 2r_5 + r_9 - k_0[\mathrm{HBrO_2}] \quad (23)$$

$$\frac{d[\mathrm{BrO_3^-}]}{dt} = -r_1 + r_5 - r_9 + k_0\left([\mathrm{KBrO_3}]^{IN} - [\ \mathrm{BrO_3^-}]\right) \quad (24)$$

$$\frac{d[\mathrm{SO_3^{2-}}]}{dt} = -r_7 + r_8 + k_0\left([\mathrm{Na_2SO_3}]^{IN} - [\ \mathrm{SO_3^{2-}}]\right) \quad (25)$$

$$\frac{d[\mathrm{HSO_3^-}]}{dt} = -r_1 - r_6 + r_7 - r_8 - k_0[\mathrm{HSO_3^-}] \quad (26)$$

$$\frac{d[\mathrm{Fe(CN)_6^{4-}}]}{dt} = -2r_9 + k_0\left([\mathrm{K_4Fe(CN)_6}]^{IN} - [\mathrm{Fe(CN)_6^{4-}}]\right) \quad (27)$$

$$\frac{d[\mathrm{Fe(CN)_6^{3-}}]}{dt} = 2r_9 - k_0[\mathrm{Fe(CN)_6^{3-}}] \quad (28)$$

$$\frac{d[\mathrm{H}^+]}{dt} = -r_2 - r_3 + r_4 + r_5 + 3r_6 - r_7 + r_8 - 3r_9 + r_{10} + k_0\left([\mathrm{H}^+]^{IN} - [\mathrm{H}^+]\right), \quad (29)$$

where k_0 is the feeding rate, $[\mathrm{I}]^{IN}$ is the concentration of species I being injected in the CSTR. $[\mathrm{H}^+]$ is being injected as $\mathrm{H_2SO_4}$, an acid with $p\mathrm{K}_{a,1} = -3$ and $p\mathrm{K}_{a,2} = 2$. The lowest pH of the oscillator being about 2, we can consider that $\mathrm{H_2SO_4}$ exists in solution only as species $\mathrm{HSO_4^-}$ and $\mathrm{SO_4^{2-}}$. At a given time, for a proton concentration in the reactor $[\mathrm{H}^+]$, an injection of $[\mathrm{H_2SO_4}]^{IN}$ results in an injected concentration of protons given by

$$[\mathrm{H}^+]^{IN} = [\mathrm{H_2SO_4}]^{IN}\left(1 + \frac{1}{(1 + [\mathrm{H}^+]/K_{a,2})}\right). \quad (30)$$

We consider here that the protonation equilibra of $\mathrm{H_2SO_4}$ are infinitely fast compared with reactions 1 to 9. We do neglect the contribution of protons coming from a remaining quantity of $\mathrm{HSO_4^-}$ at low pH that would liberate protons when the pH rises in the reactor.

Equations (20) to (29) take the form of Equation 1 in the Main Text, that we reproduce here for clarity,

$$\frac{dC_i(t)}{dt} = f_i\left(k_j, C_l(t)\right) + k_0\left(C_i^{IN} - C_i(t)\right). \quad (31)$$

The system of equations (20) to (29) can be simulated in a macroscopic CSTR as is. In contrast, to simulate these equations in a μCSTR we need to take into account the digital character of the injection. For each species i, (31) was rewritten as

$$\frac{dC_i(t)}{dt} = \chi(1 - H)f_i\left(k_j, C_l(t)\right) + H\frac{k_0}{t_{inj}}\left(C_i^{IN} - C_i(t)\right), \quad (32)$$

where H is a function that takes into account the digital character of the injection. It is equal to 1 during the injection phase, that lasted $t_{inj} = 5$ s in our simulations, and equal to 0 otherwise. Note

that this implementation assumes perfect mixing as soon as the injection phase ends. χ is a coupling parameter that we have added to remove a divergence due to the sharp change in the derivative introduced by the discontinuous function H. After an injection, the concentrations of the different species may change quite abruptly and make the computed derivative very large, thus introducing, for instance, negative values of the concentrations. To smooth this effect, the contribution of $f_i\left(k_j, C_l(t)\right)$ to (32) was switched on linearly after an injection, with $\chi = t/t_{swicth}$, and $t_{switch} = 10$ s.

Differential equations were solved in Matlab using `ode23s` solver for stiff problems. It is a one-step solver that uses a modified Rosenbrock formula of order 2.

6.2 Comparison experiments/simulations in a closed reactor

The experimental and simulated phase diagram of the Edblom oscillator in the same conditions (5 mM H_2SO_4, 20 mM $K_4[Fe(CN)_6]$, and 65 mM $KBrO_3$), displayed in Figure 11, are significantly different. Several reasons can be invoked to explain this discrepacy: i) mixing in the experiments takes 7 s, while in the simulations it is instantaneous, ii) injection and mixing are considered independent processes in the simulations, but they are simultaneous, and coupled to spatial transport, in the experiments, iii) the high surface to volume ratio of the μCSTR is not taken into account in the simulations, notably the evaporation of important intermediates such as Br_2 through the porous walls of PDMS, and iv) the influence of the fluorescent dye is disregarded in the simulations. Instead of studying each of these processes in detail we decided to take a phenomenological description. To do so we performed a series of experiments, and the corresponding simulations, using the μCSTR as a closed reactor for different concentrations of H_2SO_4 and Na_2SO_3. In these experiments the four reagents were injected 50 consecutive times into the annular reactor and mixed to create a reproducible initial condition corresponding to 1/4 of the volume of the reactor for each injected solution. The injection valves were closed, mixing remained active and fluorescence was recorded. The results are displayed in Figure 12. For all the experiments the fluorescence intensity (the pH) stays high and stable until it abruptly drops (within 30 s) and remains low. The time at which the fluorescence (pH) drops depends on $[Na_2SO_3]$ and $[H_2SO_4]$. The behavior of the Edblom oscillator at 5 mM H_2SO_4 in a closed reactor is significantly different for the experiments and the simulations. In contrast, results are similar when we compare simulations and experiments at 10 and 5 mM H_2SO_4 respectively. We argue that increasing the concentration of H_2SO_4 in the simulations to 10 mM phenomenologically takes into account the factors evoked above that are not incroporated in the simulations. We thus compare, in the Figure 5 of the Main Text, the experimental phase diagram at 5 mM H_2SO_4 with the simulated phase diagram at 10 mM H_2SO_4 .

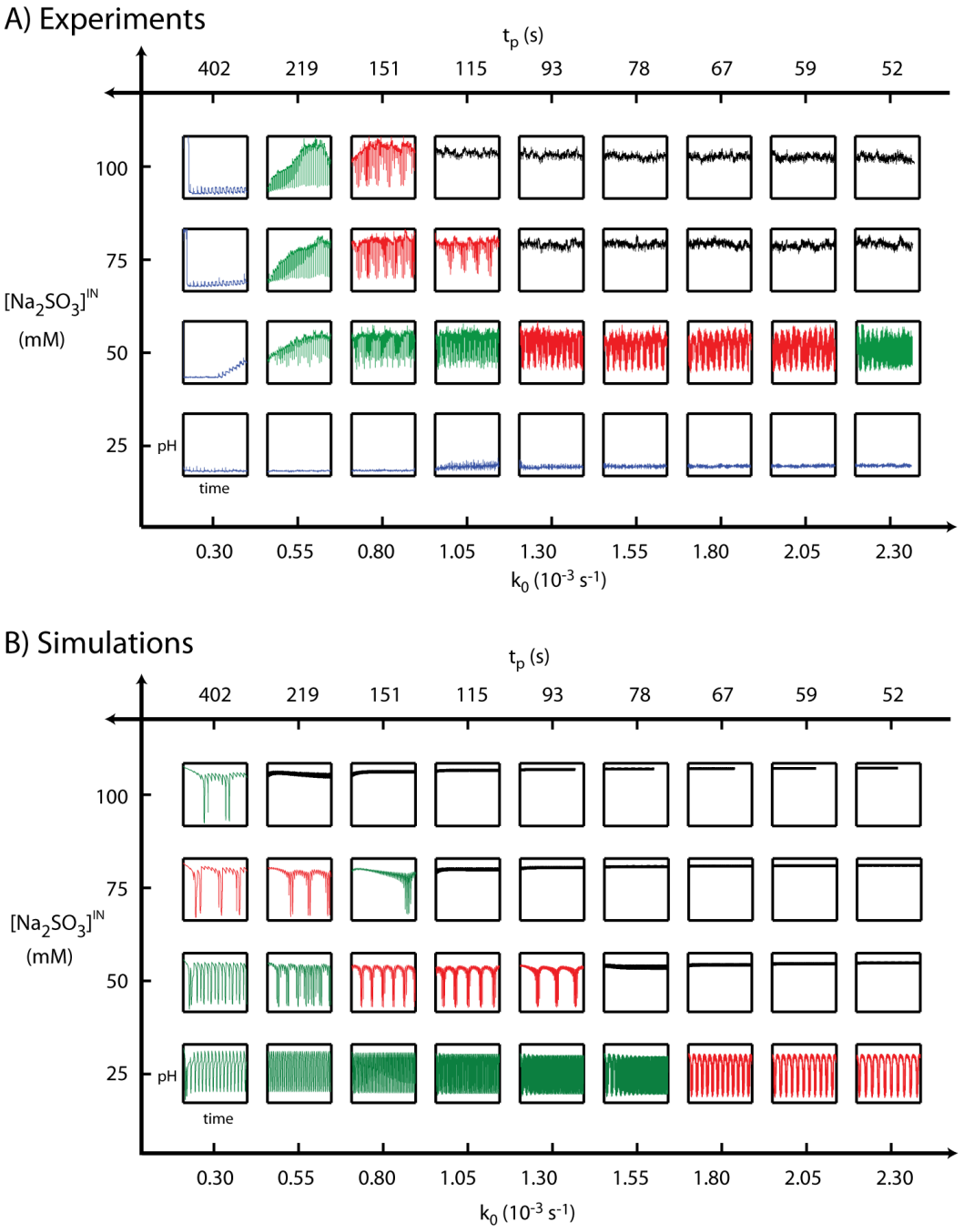

Figure S 11: Experimental (top) and simulated (bottom) phase diagram of the Edblom oscillator in the μCSTR for different Na_2SO_3 input concentrations and at different feeding rates k_0 (and their corresponding injection periods t_p). Each square represents pH *vs.* time during a 2 h experiment. Time traces are colour-coded according to the observed steady state: low pH (blue), forced oscillations (green), sustained oscillations (red), and high pH (black). In contrast with Fig. 5 in the Main Text, here [H2SO4] = 5 mM both for the experiment and for the simulations. The remaining injected concentrations are $K_4[Fe(CN)_6]$ 20 mM and $KBrO_3$ 65 mM.

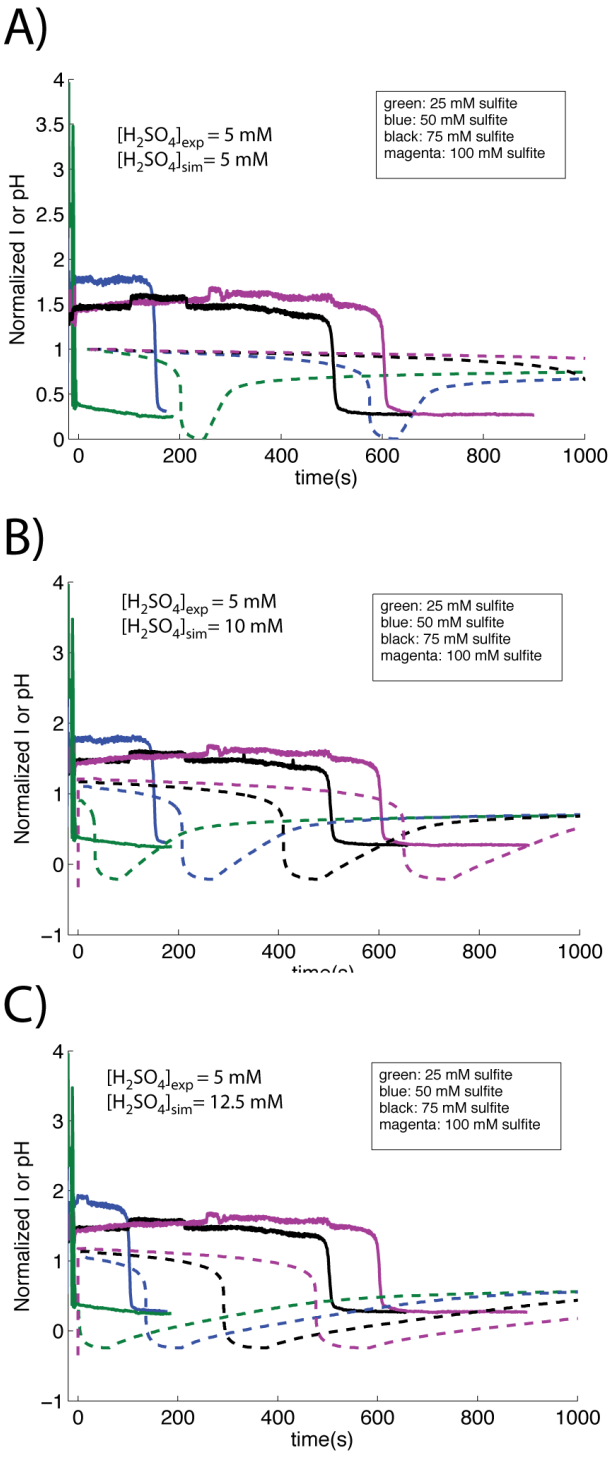

Figure S 12: Normalized intensity (experiments, solid lines) or normalized *p*H (simulations, dashed lines) *vs* time after mixing in a closed reactor for different concentrations of Na_2SO_3 (25 mM, green, 50 mM, blue, 75 mM, black, and 100 mM, magenta) and H_2SO, and for 20 mM $K_4[Fe(CN)_6]$ and 65 mM $KBrO_3$.

6.3 Simulated *p*H *vs* time plots

In this subsection are displayed, in large format, the normalized *p*H *vs* time plots represented in the phase diagram in Fig. 5B in the Main Text. The following conditions are common to all graphs: $[H_2SO_4]$ = 10 mM, $K_4[Fe(CN)_6]$ 20 mM and $KBrO_3$. 65 mM. The graphs are color-coded as in the Main Text: low *p*H (black), forced oscillations (green), sustained oscillations (red), high *p*H (black).

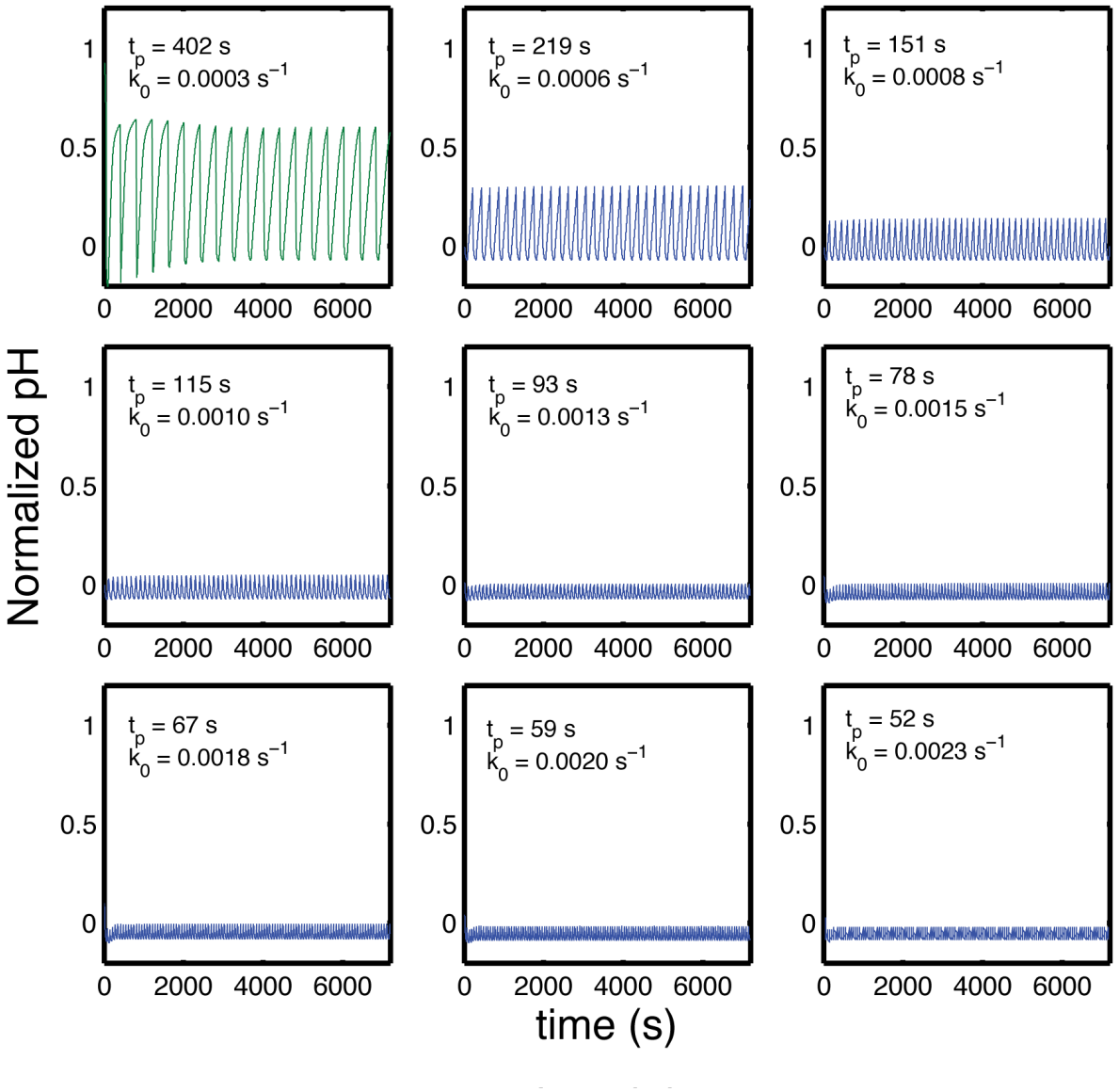

Figure S 13: Simulated normalized average fluorescence intensity for different injection periods, t_p, and their corresponding feeding rates, k_0 when the concentration of injected Na_2SO_3 was 25 mM.

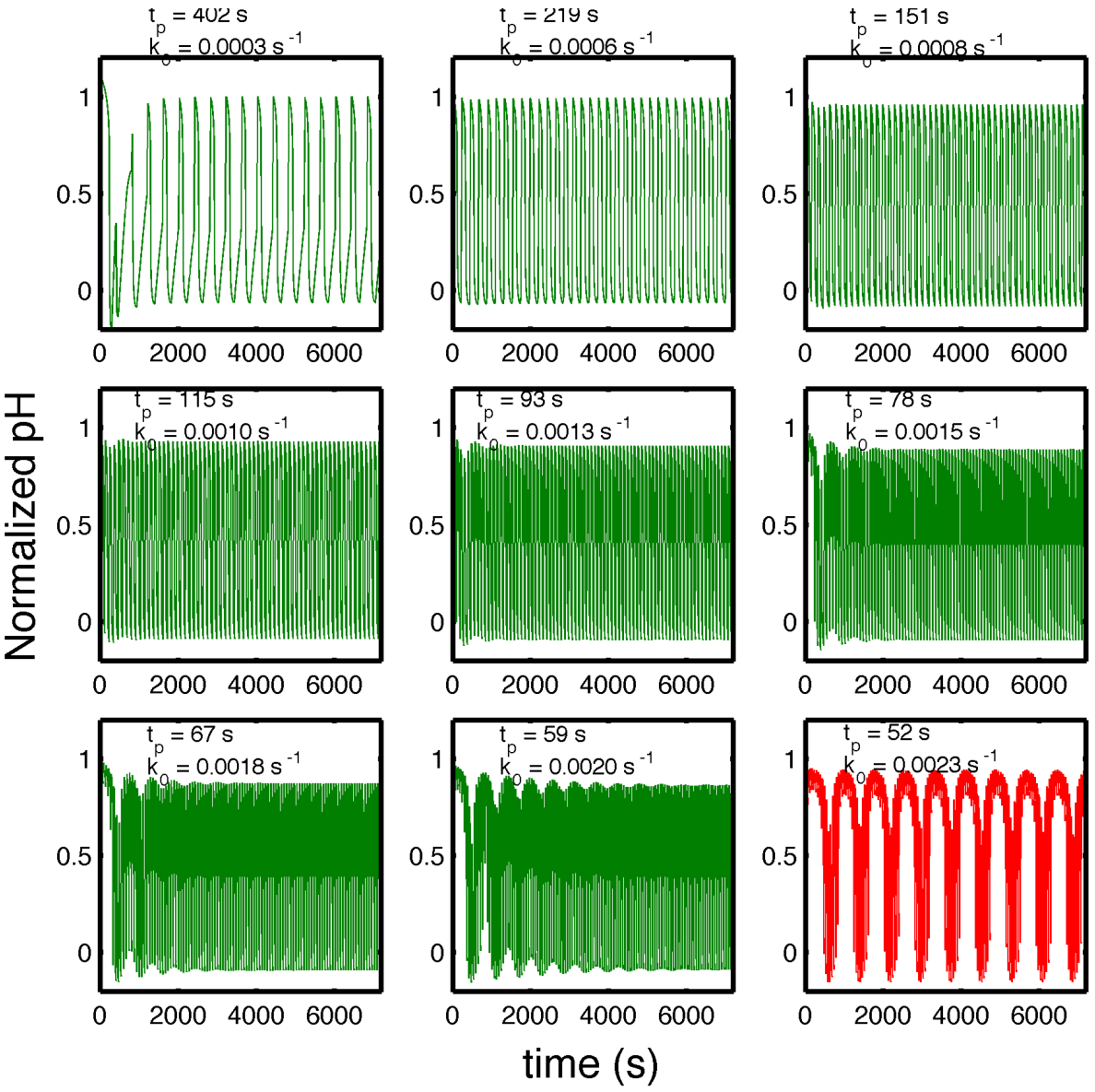

Figure S 14: Simulated normalized average fluorescence intensity for different injection periods, t_p, and their corresponding feeding rates, k_0 when the concentration of injected Na_2SO_3 was 50 mM.

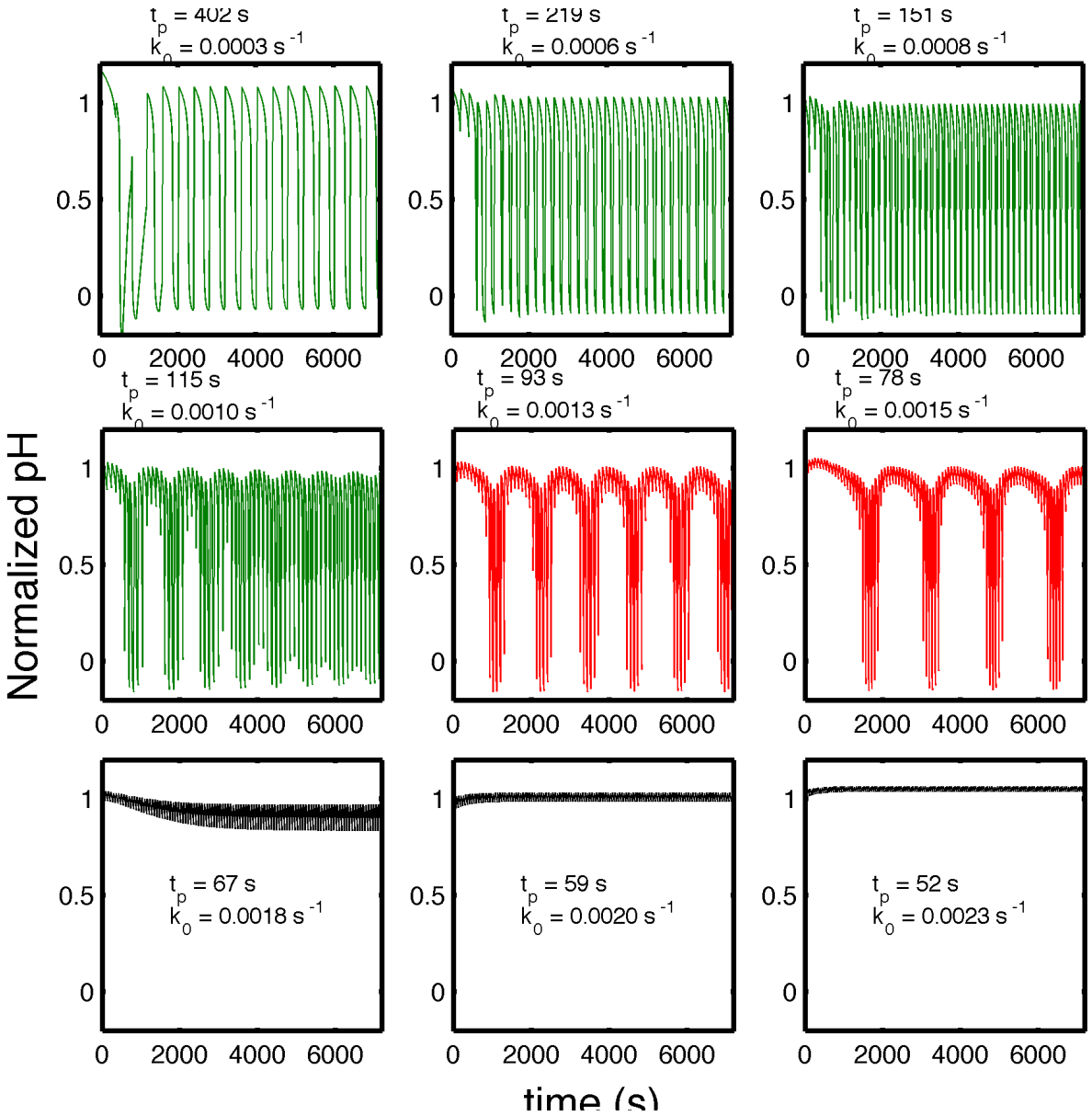

Figure S 15: Simulated normalized average fluorescence intensity for different injection periods, t_p, and their corresponding feeding rates, k_0 when the concentration of injected Na_2SO_3 was 75 mM.

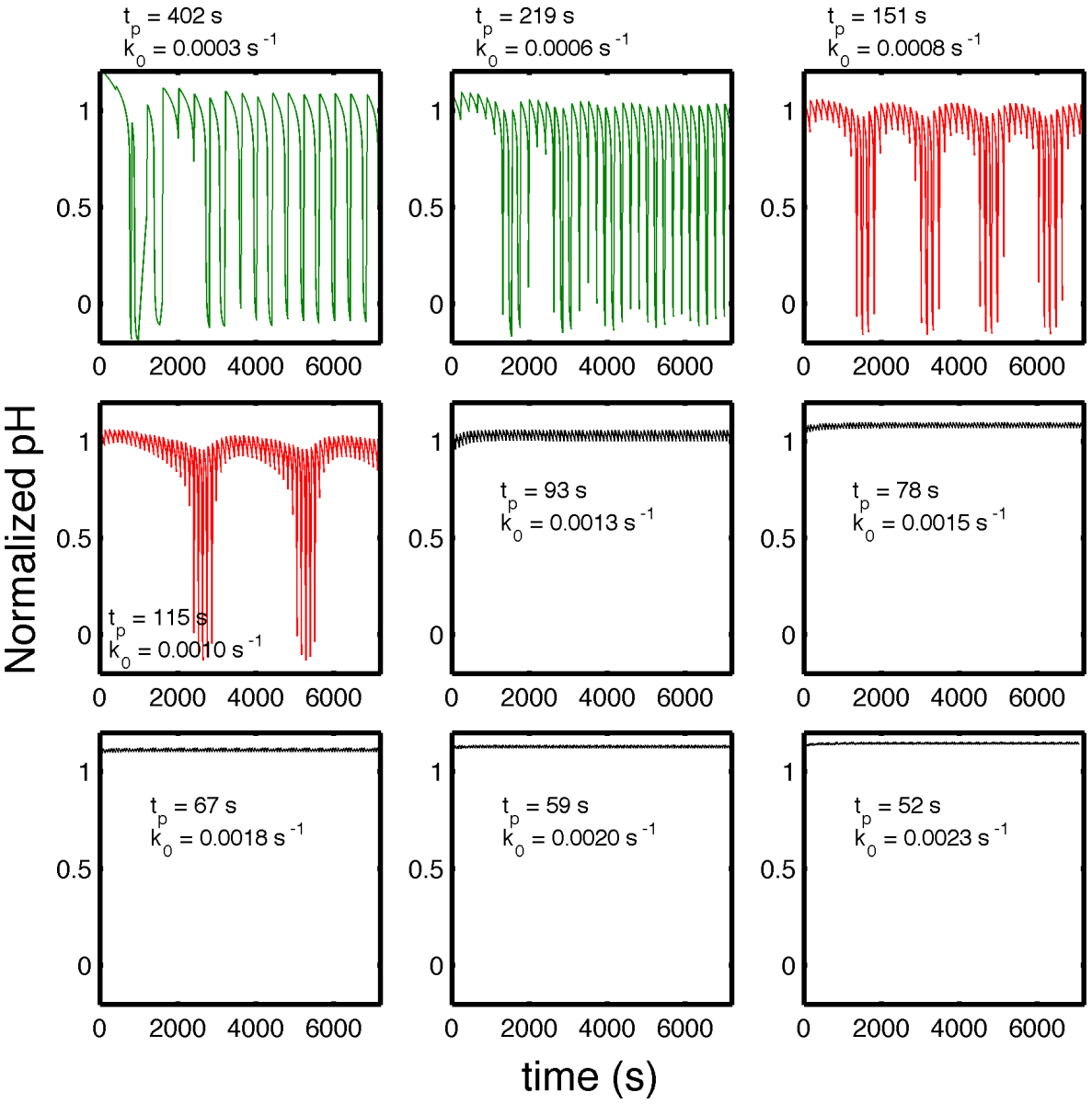

Figure S 16: Simulated normalized average fluorescence intensity for different injection periods, t_p, and their corresponding feeding rates, k_0 when the concentration of injected Na_2SO_3 was 100 mM.

7 Attached files

7.1 Video of the Edblom oscillator in the μCSTR

A video showing two periods of the Edblom oscillator for 20 mM $K_4[Fe(CN)_6]$, 65 mM $KBrO_3$, 75 mM Na_2SO_3, and 5 mM H_2SO_4 being injected, with a period $t_p = 115$ s, in the μCSTR and observed with 10μM Oregon green under a fluorescence microscope is available for download.

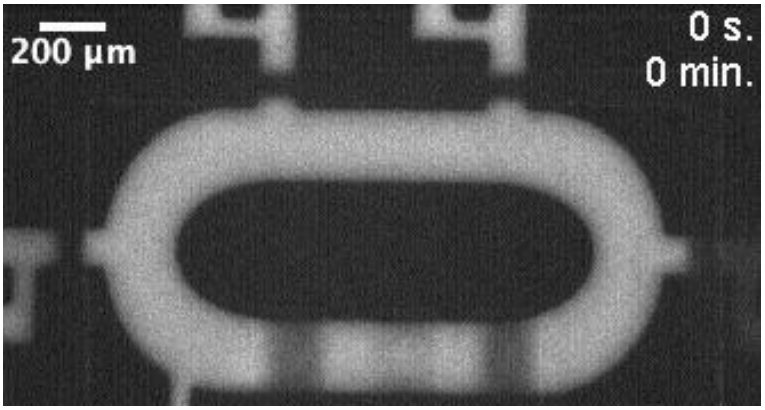

Figure S 17: First frame of the attached video.

7.2 Matlab code for simulations

The Matlab code for the simulations described in section 6 is available for download. It is constituted of the following functions:

```
function do_solve_Edblom_kinetics_for_several_input
% Calls the solver plot_solutions_parameter_Edblom_kinetics for
%different concentrations of sulfite and sulfuric acid

function plot_solutions_parameter_Edblom_kinetics(varargin)
%Calls the ODE solver function solve_kinetics_with_parameters_CSTR_Edblom( pumpingPeriod(i),
%fId ) for different values of pumpingPeriod.  Then makes plots with the
%results from that function.  'param' and 'out' are the principal
%structures, with the parameters and the output values
%If varargin > 0 the first one is the input sulfite conc and the second one
%the input sulfuric acid conc

function [t y] = solve_kinetics_with_parameters_CSTR_Edblom(param, x0, iCondition)
% This function implements the kinetic model for the pH oscillator in a CSTR described
%in Edblom, JPhysChem 1989, Table 1
%in a continuous or digital CSTR modeled through k0
%Input is a structure param with the rate constants and the file id fId to write
%results in a text file, x0 is a vector containing the initial conditions,
%'iCondition' is a counter for an experiment with different k0
%OUPUT are vectors time 't' and solution of the
%ODE 'y' as well as the structure param with normalized rates sigmai

function param = create_parameter_struct_Edblom()
% Initializes the structure 'param' which stocks all the relevant parameters
%set by the user to solve the ODEs

function out = create_output_struct_Edblom()
% Initializes the structure 'out' which stocks all the quantities
%computed during the simulation
```

```
function jacob = edblom_jacobian(x, rate, H, chemCoupling, k0Comp)
% Claculates the Jacobian matrix of the Edblom ODE system
% written in function solve_kinetics_with_parameters_CSTR_Edblom
% INPUT: 'x' vector of concentrations, 'rate' structure of rates
% 'H' equal to 0 or 1 depending on injection conditions, 'cte'
% equal to 1 or 2 for digital or continuous injection,
% 'k0Comp' computed k0 value

function plot_Edblom_data(out, param)
% Plots outputs from function plot_solutions_parameter_Edblom_kinetics
% out and param are structures defined in that function
```